(2)

NAVAL POSTGRADUATE SCHOOL
Monterey, California

THESIS

Evaluation of a Potential Wave Division Multiplexer (WDM)

for Use in the IRSTD

by

Paul Thomas Ferman

December 1989

Thesis Advisor: David D. Cleary

REPORT DOCUMENTATION PAGE

REPORT SECURITY CLASSIFICATION: UNCLASSIFIED	1b RESTRICTIVE MARKINGS
SECURITY CLASSIFICATION AUTHORITY	3. DISTRIBUTION / AVAILABILITY OF REPORT: Approved for public release; distribution unlimited.
DECLASSIFICATION / DOWNGRADING SCHEDULE	
PERFORMING ORGANIZATION REPORT NUMBER(S)	5. MONITORING ORGANIZATION REPORT NUMBER(S)
NAME OF PERFORMING ORGANIZATION: Naval Postgraduate School; 6b. OFFICE SYMBOL (If applicable): 33	7a. NAME OF MONITORING ORGANIZATION: Naval Postgraduate School
ADDRESS (City, State, and ZIP Code): Monterey, CA 93943-5000	7b. ADDRESS (City, State, and ZIP Code): Monterey, CA 93943-5000
NAME OF FUNDING / SPONSORING ORGANIZATION; 8b. OFFICE SYMBOL (If applicable)	9. PROCUREMENT INSTRUMENT IDENTIFICATION NUMBER
ADDRESS (City, State, and ZIP Code)	10 SOURCE OF FUNDING NUMBERS: PROGRAM ELEMENT NO. / PROJECT NO. / TASK NO / WORK UNIT ACCESSION NO.

TITLE (Include Security Classification): EVALUATION OF A POTENTIAL WAVE DIVISION MULTIPLEXER FOR USE IN THE IRSTD

PERSONAL AUTHOR(S): Fernan, Paul T.

TYPE OF REPORT	13b. TIME COVERED	14. DATE OF REPORT (Year, Month, Day)	15 PAGE COUNT
Master's Thesis	FROM _____ TO _____	December 1989	61

SUPPLEMENTARY NOTATION: The views expressed in this thesis are those of the author and do not reflect the official policy or position of the Department of Defense or U.S. Government

COSATI CODES		
FIELD	GROUP	SUB-GROUP

18. SUBJECT TERMS (~~Continue on reverse if necessary and identify by block number~~): Wave Division Multiplexing; ~~IRSTD~~; Fiber Optics.

ABSTRACT (Continue on reverse if necessary and identify by block number)

The design of a Wave Division Multiplexer (WDM) was evaluated. This design could be used in the AN/SAR-8 infrared search and target designation system currently being developed by the Navy. The design featured a spherical grating with a radius of curvature of 115mm to test the capability of multiplexing 180 channels. The grating was able to couple light from laser diodes at four different wavelengths (780.0nm, 789.0nm, 848.0nm and 849.0nm). The most significant factor in coupling efficiency was astigmatism. This decreased the demultiplexing coupling efficiency by a factor of 500. The source linewidths were measured to assess the possibility of wavelength slicing. The capability to multiplex 180 channels is possible but cannot yet be achieved due to the lack of light sources that cover the wavelength range required for a 180 channel system.

DISTRIBUTION / AVAILABILITY OF ABSTRACT: ☐ UNCLASSIFIED/UNLIMITED X SAME AS RPT. ☐ DTIC USERS	21. ABSTRACT SECURITY CLASSIFICATION: UNCLASSIFIED
NAME OF RESPONSIBLE INDIVIDUAL: David D. Cleary	22b. TELEPHONE (Include Area Code): (408) 646-2828; 22c. OFFICE SYMBOL: 61-Cl

FORM 1473, 84 MAR — 83 APR edition may be used until exhausted. All other editions are obsolete

SECURITY CLASSIFICATION OF THIS PAGE

U.S. Government Printing Office: 1986—606-243

Approved for public release; distribution is unlimited.

Evaluation of a Potential Wave Division Multiplexer (WDM) for Use in the IRSTD.

by

Paul Thomas Fernan
Lieutenant , United States Navy
B.S.E.E., United States Naval Academy, 1983

Submitted in partial fulfillment of the requirements for the degree of

MASTER OF SCIENCE IN PHYSICS

from the

NAVAL POSTGRADUATE SCHOOL
December 1989

Author: Paul Thomas Fernan
Paul Thomas Fernan

Approved by:
David D. Cleary, Thesis Advisor

Alfred W. M. Cooper, Second Reader

Karlheinz E. Woehler, Chairman, Department of Physics

ABSTRACT

The design of a Wave Division Multiplexer (WDM) was evaluated. This design could be used in the AN/SAR-8 infrared search and target designation system currently being developed by the Navy. The design featured a spherical grating with a radius of curvature of 115mm to test the capability of multiplexing 180 channels. The grating was able to couple light from laser diodes at four different wavelengths (780.0nm, 789.0nm, 848.0nm and 849.0nm). The most significant factor in coupling efficiency was astigmatism. This decreased the demultiplexing coupling efficiency by a factor of 500. The source linewidths were measured to assess the possibility of wavelength slicing. The capability to multiplex 180 channels is possible but cannot yet be achieved due to the lack of light sources that cover the wavelength range required for a 180 channel system.

TABLE OF CONTENTS

I. INTRODUCTION

A. MOTIVATION

The AN/SAR-8 is an infrared search and target designation system being developed for use in the U.S. Navy. The advance design model Infrared Search and Target Designation System (IRSTD) is used for research at the Naval Postgraduate School. It has a 180 detector vertical array mounted in a rotating head to provide 360^0 coverage of the horizon. It must transfer a large amount of data from the rotating head to the stationary base for analysis. The IRSTD currently uses a series of concentric slip rings to maintain continuous signal transmission across the rotational interface. Electrical slip rings are relatively straightforward as data integrity can be maintained through brushes which contact the metal rings.

One of the disadvantages, however, of slip rings is that physical contact must be maintained between the stationary and rotating assemblies. A fiber optic rotary joint can be used to eliminate the need for such contact. Fiber optics also have many advantages over copper wire as a transmission medium. The advantages include a large bandwidth (data capacity), immunity to radio-frequency or electromagnetic interference, absence of spark hazards, low bulk and weight and absence of unwanted radiation.

Three components are involved in the use of fiber optics to pass information across a rotational interface: a rotating fiber, a stationary fiber and a mechanical assembly to maintain the alignment of the two. In the case of continuous data transmission the alignment of the two fibers must be maintained through all degrees of rotation. The simplest and most direct method to accomplish this is to place the transmitting and receiving fibers on the axis of rotation of the mechanical assembly. Because only one fiber can be placed on the axis of rotation, some means of multiplexing is required.

The use of an optical rotary joint allows for not only for conventional time division multiplexing (TDM) but also wave division multiplexing (WDM). Unlike TDM, uninterrupted data flow can be maintained for all 180 detectors with the use of WDM. Several WDM designs exist, however none have the capability to multiplex the 180 channels required for the IRSTD. This thesis investigates the possible design of a WDM system that has the performance of existing systems and the ability to multiplex 180 channels for use in the IRSTD.

B. BACKGROUND

In wave division multiplexing, or optical multiplexing, different wavelengths of light are transmitted simultaneously in the same fiber. Each different wavelength is encoded with information and then focused onto the end of the optical fiber by a diffraction grating for transmission. Another grating at the receiving end separates the transmitted light into its constituent wavelengths for information retrieval. Several schemes of optical multiplexing have been investigated, with blazed gratings showing the most promise [Tomlinson 1977].

Designs featuring plane gratings use lenses to collimate and focus the reflected light onto the receiving fibers [Aoyama and Minowa 1979]. The lenses in these designs are separate from the grating, making it difficult to maintain proper system alignment. In an effort to simplify alignment, research has been conducted using graded-index refraction (GRIN) rods to focus the reflected light [Lipson and Harvey 1983, Tomlinson and Lin 1978]. The fiber arrays can be cemented to the GRIN lens which is then cemented to the grating once alignment has been achieved.

In an effort to remove collimating and focusing lenses altogether, systems have been designed using a concave grating to reflect and focus the light simultaneously. The

fiber arrays can then be cemented into a slab wave guide to maintain alignment and provide protection to the fibers [Watanabe and Nosu 1980]. The waveguide can also be used to curve a thin plane grating to provide focusing ability [Fujii and Minowa 1981].

Concurrent with the research into various grating designs was the drive to increase the number of channels that could be multiplexed. As of 1984, several systems had demonstrated the ability to multiplex between 8 and 28 channels [Hendricks 1984]. Refinements of the gratings used have been accomplished by various researchers, with most of the current research concentrated on smaller radii of curvature and aberration correction. Aberration correction reduces the astigmatism of the grating and increases coupling efficiency. An aberration corrected grating with a radius of curvature of 50mm has achieved a coupling efficiency of 55% compared with 10% efficiency for a grating without aberration correction [Harada and Kita 1983]. A 10 channel demultiplexer has been manufactured using a 50mm aberration corrected grating [Watanabe and Nosu 1980].

Wave division multiplexing is a proven method of increasing the information capacity of an optical fiber. Unfortunately, the number of channels that can be multiplexed depends on radius of curvature of the grating. To multiplex the 180 channels of the IRSTD requires a radius of curvature greater than 50mm. Assuming typical performance criteria, it is believed that a grating with a 115mm radius of curvature could be used to multiplex 180 channels. This thesis evaluates the feasibility of using a system with this grating for wave division multiplexing.

C. THESIS OUTLINE

The thesis is divided into six chapters. Chapter I is the introductory chapter and provides the motivation for the thesis and a brief history of wave division multiplexer design. Chapters II and III provide an overview of the optical concepts important in the

understanding of grating behavior and the development of the mathematics used in concave grating theory. Chapter IV contains information on the components used in the experiment and describes the setup and procedures of the design analysis. Chapter V contains the results of the experiment . The final chapter, Chapter VI, evaluates the feasibility of the envisioned design and makes recommendations for improvement of the design. Suggestions for further research are also contained in Chapter VI.

II. FUNDAMENTALS OF OPTICS

Multiplexing can be accomplished with a spherical grating because of the interference pattern produced when incident light is reflected from the grating. A thorough understanding of how the pattern is formed is necessary to design an effective multiplexing system. This chapter briefly discusses the key concepts useful in understanding the interference pattern produced by a spherical grating.

A. INTERFERENCE OF TWO POINT SOURCES

The wavefronts of two point sources will overlap in space. When the sources are the same wavelength the interference of their wavefronts will form a characteristic pattern. In the far field, or Fraunhofer region, the separation of the sources is negligible compared to the distance to the point of observation. At various points in space, the total irradiance can be greater, less than, or equal to the the sum of the irradiance of the two sources. The total irradiance at a point in space is dependent upon the phase difference between the wavefronts of the two sources at that point. For two point sources separated by a distance, a, the phase difference, α, equals $(ka/2)\sin\theta$ where $k = 2\pi/\lambda$ and θ is the angle to the point of observation measured from a line perpendicular to the two points. It can be shown that the irradiance as a function of phase difference is

$$I = 4I_0\cos^2\alpha. \tag{2.1}$$

where the individual intensity of each source is I_0 and α is the phase difference between wavefronts at a point in space.

B. INTERFERENCE OF MANY SOURCES

Increasing the number of sources from two to an arbitrary number, N, requires a modification of Equation 2.1. Again, the electric field at a point in space is calculated by

summing the individual contributions of each source. The resultant total electric field can be squared to give an expression of the intensity as a function of phase difference,

$$I = I_0\left(\frac{\sin N\alpha}{\sin\alpha}\right)^2. \tag{2.2}$$

It can be shown that at a point in space where all the emitted wavefronts are in phase ($\alpha = m\pi$), the intensity is found to be I_0N^2 where I_0 is the intensity of a single point source. Note that Equation 2.2. yields the same results as Equation 2.1 when N is set to 2.

C. SINGLE SLIT DIFFRACTION PATTERN

The diffraction pattern of light passing through a single slit can be calculated by treating the slit as a series of coherent line sources. In the far field the line source are replaced by a series of point sources across the width of the grating and located at its center. Allowing the number of point sources to approach infinity, the electric field at a point in space can be calculated by integrating the contribution due to each source. Squaring the electric field gives the measurable quantity of intensity for a single slit diffraction pattern as

$$I(\theta) = I(0)\left(\frac{\sin\beta}{\beta}\right)^2. \tag{2.3}$$

where I(0) is the peak intensity ($\theta = 0$), $\beta \equiv (kb/2)\sin\theta$, $k=2\pi/\lambda$ and b is the width of the slit. The angular dependence term $\left(\frac{\sin\beta}{\beta}\right)^2$ is often written as $\text{sinc}^2\beta$ where the sinc function is defined as $\frac{\sin\beta}{\beta}$. The angle θ is the angle from the slit to the point of observation and is measured from the normal of the grating in the plane containing the point sources. Figure 2.1 shows the Fraunhofer diffraction pattern for a single slit. The maxima occur where β is equal to an integral multiple of $\pi/2$. In terms of $\sin\theta$ then, the maxima occur when $\sin\theta = (m/2)(\lambda/b)$. This interference pattern is characteristic of all gratings and will be discussed further below.

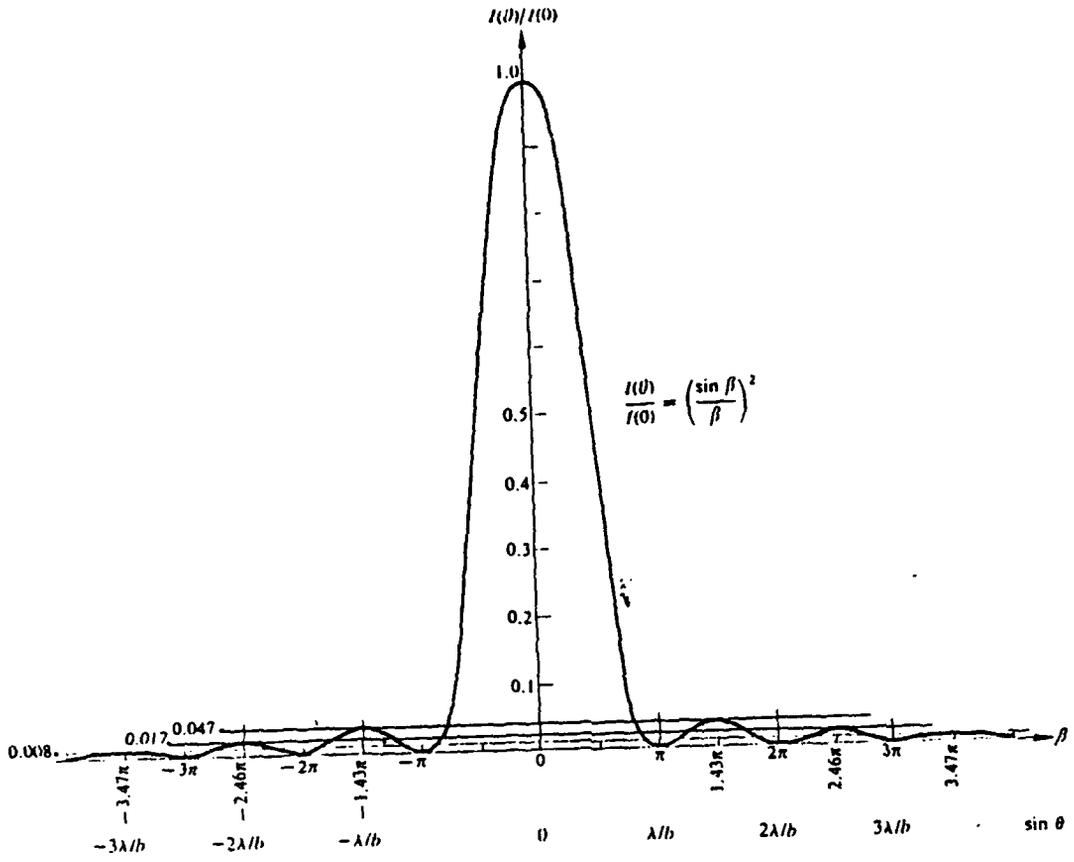

Figure 2.1 Fraunhofer diffraction pattern of a single slit

D. INTERFERENCE PATTERN OF TWO SLITS

The calculation of the interference pattern produced by light emergent from two slits is relatively straight forward given the results for a single slit and two point sources. The sources producing the interference pattern are two slits rather than two point sources. The electric field contribution of each slit at any point in space can summed and squared to give the intensity. The irradiance as a function of θ is

$$I(\theta) = 4I(0)\left(\frac{\sin\beta}{\beta}\right)^2 \cos^2\alpha \,. \qquad (2.4)$$

where I(0) is the intensity at $\theta = 0$, and α and β are defined as before.

Note that Equation 2.4 contains terms from Equation 2.1 (the interference pattern of two point sources), and Equation 2.3(the interference pattern of a single slit). The similarity of a double slit interference pattern to the superposition of a double point source pattern and a single slit pattern is seen in Figure 2.2. Instead of a series of equal intensity peaks, the pattern consists of peaks that are reduced by an amount $\text{sinc}^2\beta$. The intensity is zero at the locations when $\frac{m\lambda}{a}$ is equal to $\frac{n\lambda}{b}$ where both n and m are integers.

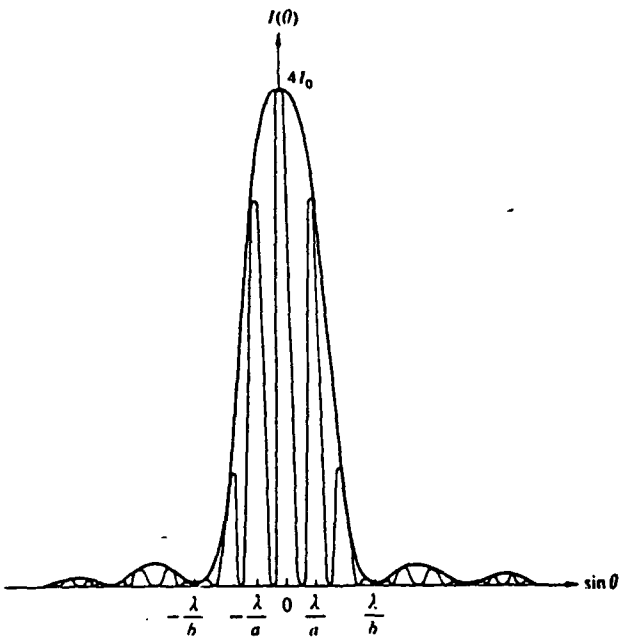

Figure 2.2 Diffraction pattern of two slits

E. INTERFERENCE OF MULTIPLE SLITS

The next pattern to be discussed is the interference pattern produced by light from a series of multiple slits. The development of the expression for the intensity of two slits is extended to encompass many slits each separated by a distance, a. The limits for the integration of the electric field contribution for light emergent from each slit are modified to

include a multitude of slits. The resulting expression for the intensity as a function of angle is

$$I(\theta) = \frac{I(0)}{N^2}\left(\frac{\sin\beta}{\beta}\right)^2\left(\frac{\sin N\alpha}{\sin\alpha}\right)^2, \qquad (2.5)$$

where N is the number of slits. That a large array of slits can be thought of as an array of many point sources grouped to form a multitude of slits is obvious from the similarity of Equation 2.5 to the expressions for the diffraction pattern of N point sources, Equation 2.2, and the diffraction pattern of two slits, Equation 2.3.

Figure 2.3 shows the interference pattern produced by multiple slits, in this case N =6. The condition for constructive interference is that one half of the phase difference between two adjacent rays, α, is an integer multiple of π. In terms of $\sin\theta$ then, the condition is $m\pi = (ka/2)\sin\theta$. This can be rewritten using $k=2\pi/\lambda$ to be $m\lambda = a\sin\theta$. It can be seen from Figure 2.3 that the maxima occur at $\sin\theta=m\lambda/a$. The maximum intensity occurs at $\theta = 0$. The succeeding local maxima (located at $m\lambda/a$) decrease in intensity as $\sin\theta$ increases. This can be explained by inspection of Equation 2.5. The quantity β is proportional to $\sin\theta$. The sine of β will change slower than β and the term $\left(\frac{\sin\beta}{\beta}\right)^2$ will decrease as $\sin\theta$ increases. As before,a zero in the intensity occurs whenever $m\lambda/a$ is an integer multiple of $n\lambda/b$.

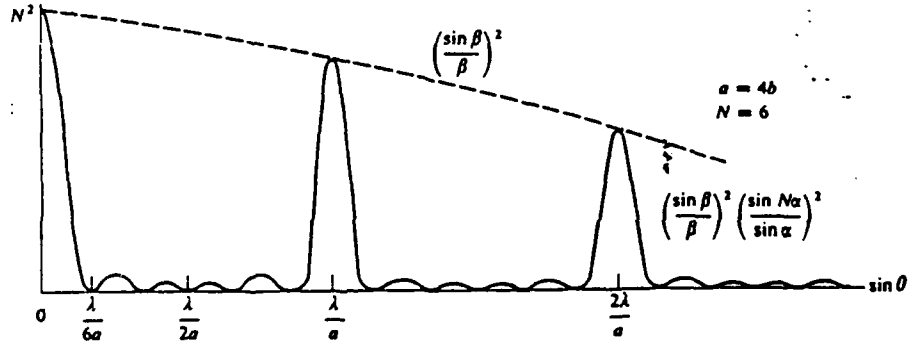

Figure 2.3 Multiple slit diffraction pattern

F. GRATINGS

Equation 2.5 can also be used to describe the interference pattern produced by light transmitted through a diffraction grating. A diffraction grating is merely a large array of evenly spaced identical slits. A grating can also be made by using small reflective elements instead of slits. A grating so manufactured is known as a reflection grating and produces the same interference pattern described by Equation 2.5. Gratings are used in a wide variety of optical instruments because of their angular dispersive properties on incident light.

Gratings are commonly illuminated at oblique angles. The condition for constructive interference of light emergent from adjacent diffracting elements must be modified for oblique angles. For light incident normal to the grating surface the condition for constructive interference of adjacent light rays is $m\lambda = a \sin\theta$, where a is the separation between elements and θ is the angle of observation as defined previously. The expression for the path difference of oblique light incident upon adjacent diffracting elements is $\lambda = a\sin\theta_i$, where θ_i is the angle of incidence. Reflection from the diffracting elements adds another difference in path length of $\lambda = a\sin\theta_r$, where θ_r is the angle of reflection. For two parallel rays of light incident at an oblique angle on adjacent diffracting elements to constructively interfere at the observation point, their path difference must be an integral multiple of wavelengths for phase matching. The condition for constructive interference is given by

$$a(\sin\theta_r - \sin\theta_i) = m\lambda. \qquad (2.6)$$

The intensity pattern of a typical grating is shown in Figure 2.4. The difference between Figure 2.3 and Figure 2.4 can be explained by the increase in the number of slits, N, in

Figure 2.4. As N increases the width of the principal maxima decreases while their relative spacing remains constant at λ/a. The subsidiary maxima between the principal maxima decrease in intensity and fade out.

A disadvantage of gratings is that the irradiance is spread over a number of low intensity spectral orders, as seen in Figure 2.4. Most of the light ends up in the zeroth order and is wasted for spectroscopic purposes, since the wavelengths of the source overlap. Most modern grating are blazed gratings. Blazed gratings are reflection gratings

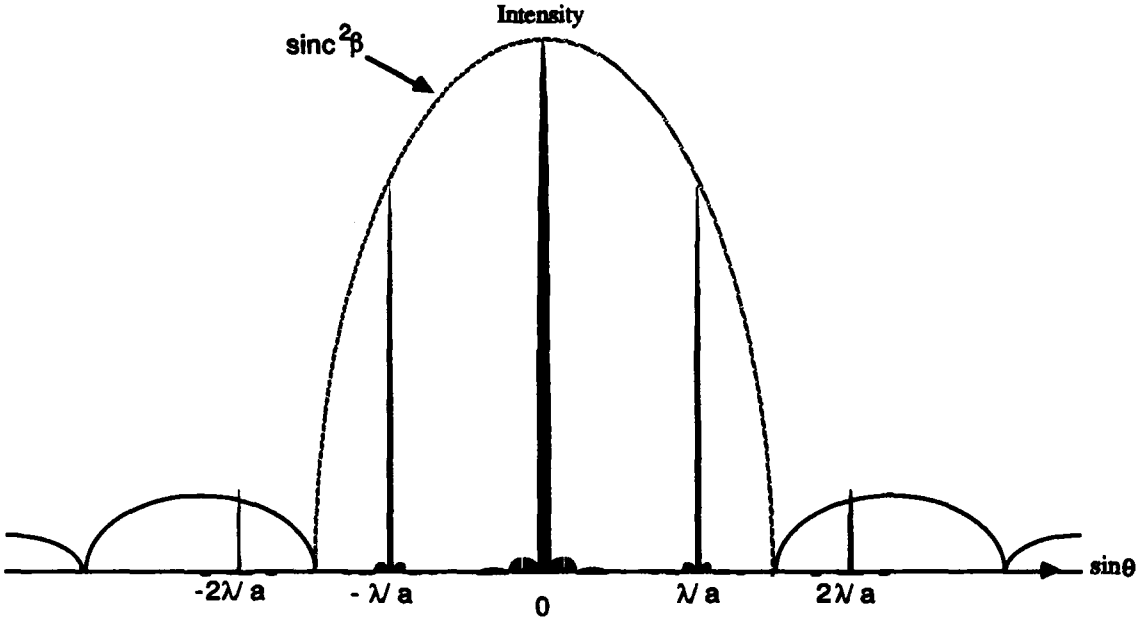

Figure 2.4 Multiple slit interference pattern

with the diffracting elements set at an angle (the blaze angle) to the grating surface. Angling the diffracting elements shifts energy out of the zeroth order into higher orders which are more useful for spectroscopic purposes.

Light incident on a blazed grating is incident at one angle with respect to the grating surface and at a different angle with respect to the surface of the diffracting elements. The

location of the peak in the single facet diffraction corresponds to specular diffraction off that face for each element and is governed by the blaze angle, γ. Figure 2.5 shows the behavior of two light rays on incident a grating blazed at angle γ.The upper rays suggest that the condition for constructive interference is unchanged because the angles are measured perpendicular to the grating surface. The lower ray in Figure 2.5 shows the case of specular reflection from a single diffracting element. These angles are measured perpendicular to the face which is at angle γ to the grating surface. For normally incident light, θ_i is equal to zero and Equation 2.6 is the same as the previous expression for the

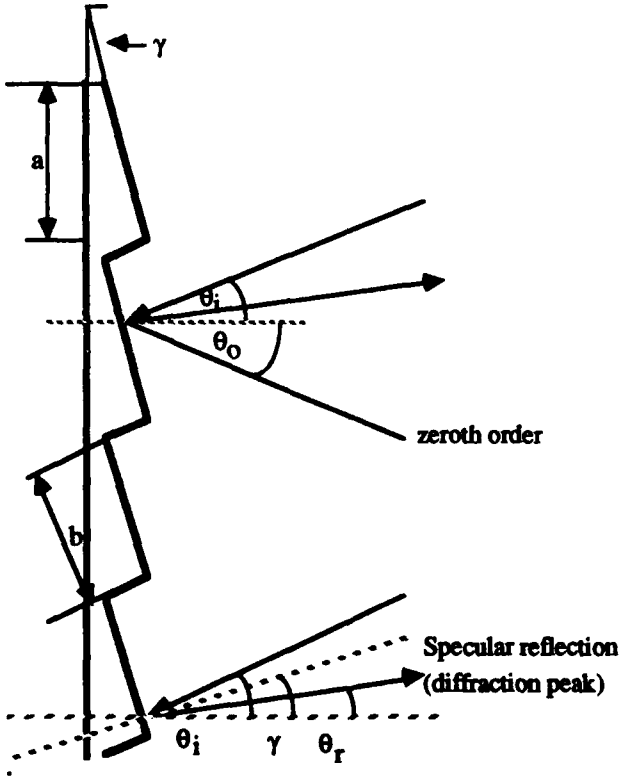

Figure 2.5 Section of a blazed reflection grating

path length difference of light incident on adjacent slits, $a\sin\theta_m = m\lambda$,with θ_m being identical to θ_r. For specular reflection off a single facet, $\theta_i - \theta_r = 2\gamma$, and in the case of

normal incidence, $\theta_r = -2\gamma$. The reflection angle is negative because both the incident ray and reflected ray are in the same side of the grating normal. Substituting θ_r in Equation 2.6 gives the expression for the path length difference for constructive interference of adjacent rays reflected from a blazed grating as

$$a \sin(-2\gamma) = m\lambda . \tag{2.7}$$

The effect of Equation 2.7 on the irradiance pattern can be seen in Figure 2.6. The $\text{sinc}^2\beta$ envelope has been shifted by an amount $\sin(-2\gamma)$. Comparing Figure 2.6 with Figure 2.4 shows that the intensity of the m=1 order has been increased, while the locations of all maxima remain fixed.shifted by $\sin(-2\gamma)$. The blaze angle, γ, can be changed to give a maximum in the first order for a given wavelength and can be varied independently of θ_m. Blazed gratings are often described in terms of a blaze wavelength rather than blaze angle.

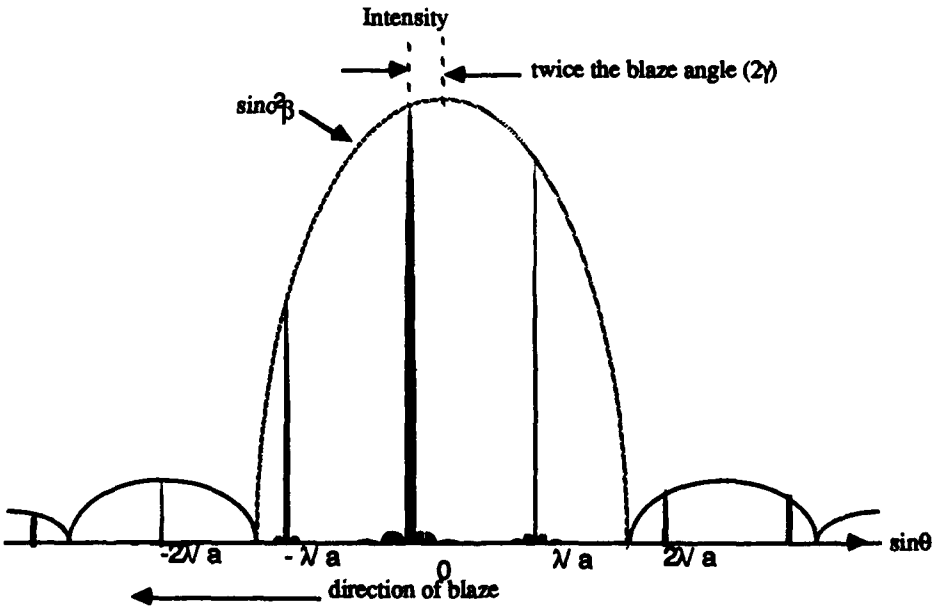

Figure 2.6 Blazed grating intensity pattern

G. SPHERICAL MIRRORS

When using a spherical grating or mirror two important aberrations occur due to the curvature of the reflecting surface. They are spherical aberration and astigmatism. Spherical aberration occurs because only rays close to the optic axis (grating normal), or paraxial rays, will be sharply focused in the focal plane. For a spherical grating the focal plane is located at a distance equal to half the radius of curvature. Figure 2.7 illustrates the effects of spherical aberration. Parallel incident rays at increasing distances, h, from the optic axis cross the optic axis inside the focal plane. If a small screen is placed at the paraxial focal plane F and then moved toward the mirror, a point is reached where the size of the circular image spot is a minimum. This disklike spot is indicated in Figure 2.7 and is called the circle of least confusion.

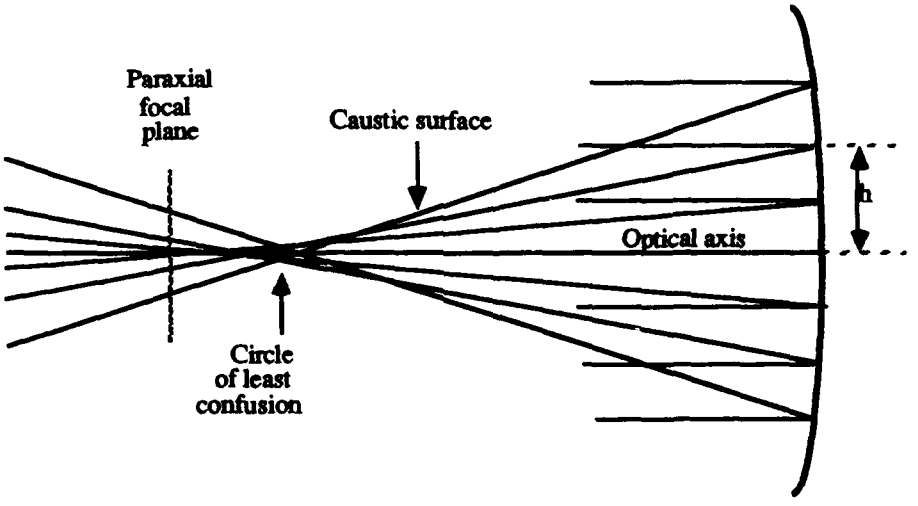

Figure 2.7 Aberration of parallel rays of light reflected from a spherical mirror

The reason for rays being focused inside the focal plane can be explained using geometric optics. All points on the surface of a spherical grating are equidistant from the center of curvature, denoted as point C in Figure 2.8. The focal point of the grating is

located at F, half the distance to the surface of the grating. A ray of light parallel to the optic axis and incident on the surface at point T is reflected and crosses the axis at X. The angle of reflection ϕ' is equal to the angle of incidence ϕ. This is equal to the angle TCA. The triangle CTX is isosceles with CX equal to XT. By inspection, CX+ XT is greater than CT. CT is the radius of curvature of the mirror which is also equal to CA. With CX equal to XT, 2CX>CA. The ray incident at T is focused at X which is inside the focal point ($CX > \frac{1}{2}CA$). The geometry of the figure shows that as T is moved toward A, the point X approaches F (the focal point), and in the limit $CX = XA = FA = \frac{1}{2}CA$.

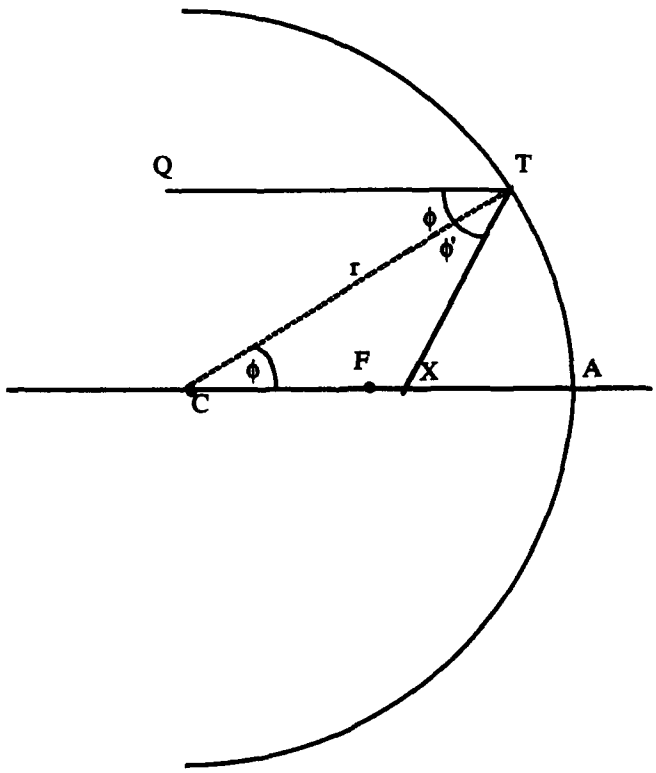

Figure 2.8 Change in focal point due to spherical aberration

The second aberration introduced with a spherical grating is astigmatism. This defect of the image occurs when an object point lies some distance from the axis of a

concave or convex mirror. The incident rays, whether parallel or not, make an appreciable angle ϕ with the mirror axis. The result is that, instead of a point image, two mutually perpendicular lines are formed. This effect is illustrated by Figure 2.9. Here the incoming rays are parallel while the reflected rays are converging toward two lines S and T. The rays in the sagittal plane are focused by the mirror into a line at S. The sagittal plane is defined as the plane containing the chief ray (the ray passing through the center of the mirror) and the optic axis. These two lines form the plane RAVE in Figure 2.9. The plane perpendicular to the sagittal plane is defined as the tangential plane, JAKE in Figure 2.9. The reflected rays in the vertical or tangential plane RAVE are seen to cross or to focus at T, while the fan of rays in the horizontal or sagittal plane JAKE cross or focus at S. If a screen is placed at E and moved toward the mirror, the image will become a vertical line at S, a circular disk at L, and a horizontal line at T.

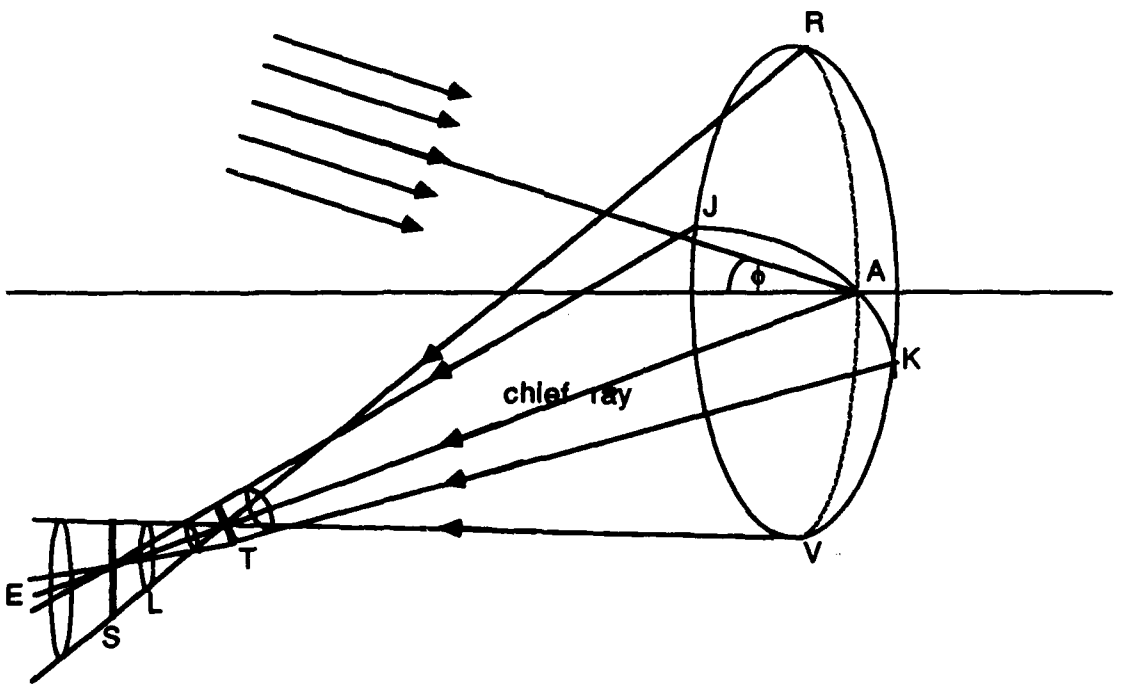

Figure 2.9 Astigmatism of a Spherical Mirror

H OPTICAL FIBERS

For completeness, a brief description of the properties of optical fibers is contained in this section. Optical fiber transmits light by means of internal reflection. Light entering the fiber is reflected off the interior surface of the fiber. Light reflected at angles greater than the critical angle is trapped in the fiber and continues to reflect down the length of the fiber. The critical angle is determined by the indices of refraction of the optical fiber and the cladding material. The cladding material protects the surface of the optical fiber and reduces light leakage.

Whether or not the light enters the fiber is determined by its angle of incidence. Light rays incident on the face of the optical fiber at angles greater than a certain value will be refracted and strike the interior surface at less than the critical angle and quickly leak out of the fiber. The maximum angle of incidence for transmission is known as the acceptance angle. The acceptance angle defines the half-angle of the acceptance cone of the fiber. The numerical aperture (NA) is the sine of this angle and is a measure of the light gathering ability of the system. It can be shown that NA is a function of the indices of refraction of the core (glass transmission medium) and the cladding of an optical fiber.

The incidence angle on the fiber face is known as the launch angle. Light incident at any angle less than the acceptance angle will be transmitted by the fiber. The actual path traveled (and the number of reflections off the interior surface of the core) is determined by the launch angle. Light entering the fiber at high angles will travel a greater path distance and undergo more reflections for a given length than will light entering at a lower angle. This can result in an appreciable difference in the arrival time of the two rays. This effect is known as intermodal dispersion.

The index of refraction of the core can be constant or vary radially in optical fibers. When the index is constant, the fiber is called stepped-index fiber. Stepped-index fiber has

high intermodal dispersion. In the case of graded index fiber, the index of the refraction of the core is decreased radially outward. The changing index of refraction of the core reduces intermodal dispersion. Rays with greater path lengths travel through material with a lower index of refraction and the arrival times of all rays are much closer than is the case for stepped index.

The final distinction between fibers is the diameter of the core and the cladding, usually expressed in microns. A 50/125 fiber has a core diameter of 50 microns and a cladding diameter of 125 microns whereas a 250/300 fiber has a core diameter of 250 microns and a cladding diameter of 300 microns. The fiber size may also depend on whether it is designed for use as multimode or single mode fiber. Multimode fibers can transmit light along several paths in the fiber depending upon the entrance angle. Single mode fibers are extremely narrow (less than 10 microns) and transmit only light that is nearly parallel to the central axis.

II. CONCAVE GRATING THEORY

In 1882 H. A. Rowland conceived the idea of combining the principle of the plane diffraction grating with the focusing properties of a spherical mirror. If a spherical grating is placed tangentially to a circle of diameter equal to the radius of curvature of the grating such that the grating center lies on the circumference, the spectrum of an illuminated point lying on the circle will be focused on this circle. This circle has come to be known as the Rowland circle. Radiation from a point, E, located on the Rowland circle will be separated upon reflection from the grating and focused at various points on the Rowland circle according to its wavelength. Figure 3.1 shows a point source composed of three wavelengths being separated and focused into three different images by the grating at the points λ_1, λ_2, and λ_3 on the Rowland circle.

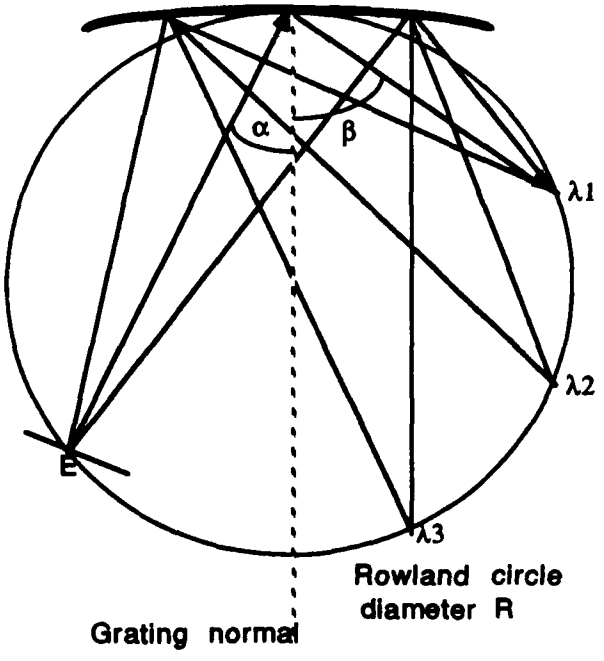

Figure 3.1 Focusing property of spherical grating

Geometric optic theory can be used to determine the focusing properties of the concave grating as well as the degree of astigmatism present. The following discussion is taken from Samson [1967]. A Cartesian coordinate system is imposed on a grating with the origin, O, located at the center of the grating. The x axis is perpendicular to the grating and the z axis is parallel to the rulings. The source point is located at A(x,y,z), the image at B(x',y',z') and a point on the grating at P(u,w,l). These points are shown in Figure 3.2.

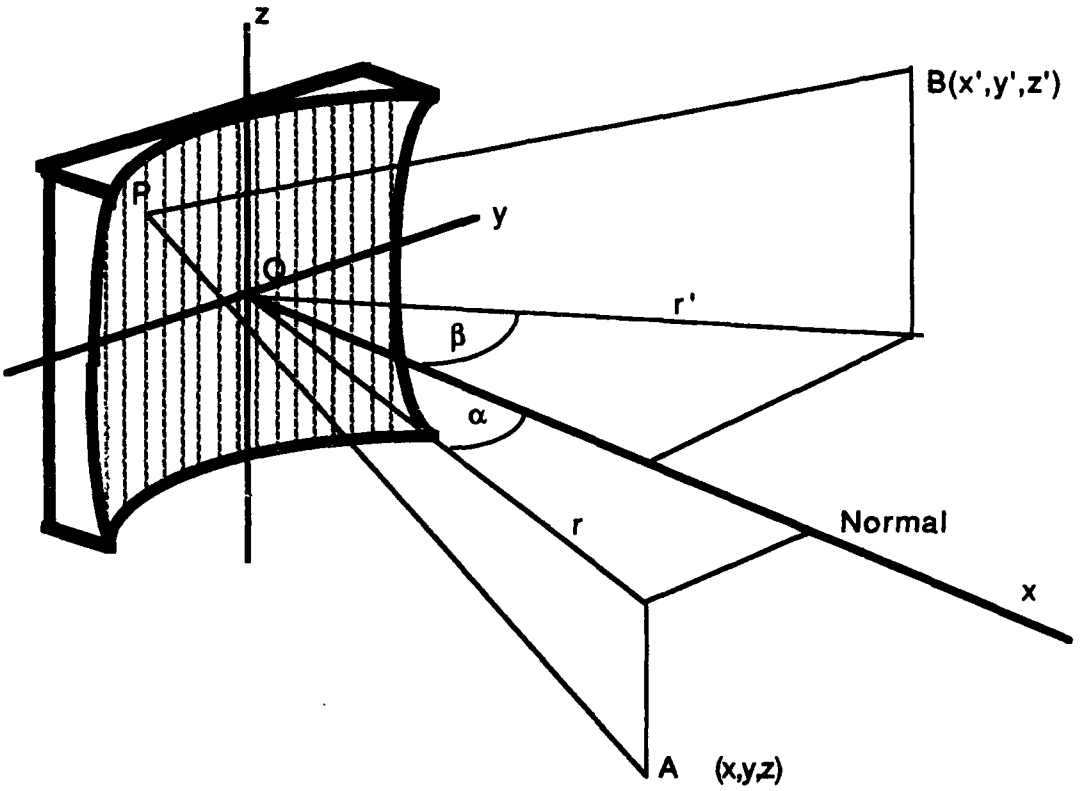

Figure 3.2 Image formation by the concave grating

An image is formed at B when the path difference of light reflected from the rulings differs by an integer multiple of wavelengths ($m\lambda$). The path difference for two rays reflected from grooves a distance w apart with a constant groove separation a is equal to $\frac{w}{a}(m\lambda)$. Constructive interference occurs when the path difference from AP to BP is an

integer number of wavelengths. It is useful to construct a path function, F, that expresses the conditions for a source at point A to image at point B.

$$F = AP + BP + \frac{w}{a}(m\lambda) \tag{3.1}$$

Having the path function F, it is possible to use Fermat's principle to determine the path that will satisfy Equation 3.1 In simple terms, Fermat's principle says that the path traversed by light from A to B will be a minimum compared to any other path. Expressing the path function in terms of the coordinates of Figure 3.2 lead to the following for the paths AP and BP:

$$(AP)^2 = (x-u)^2 + (y-w)^2 + (z-l)^2 , \tag{3.2}$$

and

$$(BP)^2 = (x'-u)^2 + (y'-w)^2 + (z'-l)^2. \tag{3.3}$$

The location of the point P is described as a function of u, w, and l. Due to the curvature of the grating, u is dependent on w and l. However, the locations of all points such as P lie on the surface of a sphere of radius R, where R is the radius of curvature of the grating. The expression for the change in u for changes in w and l is given by

$$u = R \pm [R^2 - (w^2 + l^2)]^{1/2}. \tag{3.4}$$

Only the minus sign is significant in this application. The application of Fermat's principle is simplified by converting the Cartesian coordinate system to a cylindrical one where the paths AP and BP are radial. The z axis and origin for both systems are identical. It can be seen from Figure 3.2 that $x=r\cos\alpha$, $y=r\sin\alpha$, $x'=r'\cos\beta$ and $y'=r'\sin\beta$. By converting to cylindrical coordinates and substituting Equation 3.4 for u in Equations 3.2 and 3.3, new expressions for the distance from the point P to the image and object can be developed.The binomial expansion has been used for the terms involving R. It can be shown [Samson 1967] that the resulting expressions for $(AP)^2$ and $(BP)^2$ are give by:

$$(AP)^2 = (r - w\sin\alpha)^2 + (z-l)^2 - l^2\frac{r\cos\alpha}{R} + w^2(\cos^2\alpha - \frac{r\cos\alpha}{R})$$
$$+\frac{(w^2 + l^2)^2}{4R^2}(1 - \frac{r\cos\alpha}{R})(1 + \frac{w^2 + l^2}{2R^2} + ...), \qquad (3.5)$$

and

$$(BP)^2 = (r' - w\sin\beta)^2 + (z' - l)^2 - l^2\frac{r'\cos\beta}{R} + w^2(\cos^2\beta - \frac{r'\cos\beta}{R})$$
$$+\frac{(w^2 + l^2)^2}{4R^2}(1 - \frac{r'\cos\beta}{R})(1 + \frac{w^2 + l^2}{2R^2} + ...). \qquad (3.6)$$

Taking the square root of these two equations and putting them into Equation. 3.1 will give the light path function F. According to Fermat's principle of least time, point B is located such that F will be a minimum for any point P. With A and B fixed, the only degree of freedom in the path function is the location of the point P(u,w,l) The variable u has been removed by the substitution of Equation 3.4. Therefore the path function can only vary with respect to l and w. The requirements of Fermat's principle for the path function to be a minimum can be stated mathematically as follows:

$$\frac{\partial F}{\partial l} = 0 \qquad (3.7)$$

and

$$\frac{\partial F}{\partial w} = 0 \qquad (3.8)$$

If Equations. 3.7 and 3.8 could be satisfied simultaneously for any point l and w for the fixed point B, then B would be the point of perfect focus. However, a perfect image cannot be obtained from a concave grating due to astigmatism. As in the case of a spherical concave mirror, the concave grating will image a point first into a vertical line (horizontal focus), then into a horizontal line (vertical focus). The results of Equations 3.7 and 3.8 can be used to determine the conditions for horizontal and vertical focus. It can be shown

[Samson 1967] that for B to be the best horizontal focal point (light is focused to a vertical line) the following condition must hold:

$$\frac{\cos^2\alpha}{R} - \frac{\cos\alpha}{R} + \frac{\cos^2\beta}{r'} - \frac{\cos\beta}{R} = 0. \qquad (3.9)$$

There are two solutions to this equation with the one of interest to multiplexing being:

$$r = R\cos\alpha, \qquad r' = R\cos\beta. \qquad (3.10)$$

Equation (3.10) is the equation of the Rowland circle expressed in polar coordinates. It expresses the fact that diffracted light of all wavelengths will be focused horizontally on the circumference of a circle of diameter R equal to the radius of curvature of the grating, provided that the input fiber and grating are located on the circle and the grating normal lies along a diameter.

The position of the vertical foci determine the amount of astigmatism present. Using the results of Samson [1967], the locus of the vertical foci is given by the equation

$$\frac{1}{r} - \frac{\cos\alpha}{R} + \frac{1}{r'} - \frac{\cos\beta}{R} = 0. \qquad (3.11)$$

This equation has two solutions as well, only one of which concerns multiplexing

$$r = R\cos\alpha, \qquad r' = \frac{R}{\cos\beta}. \qquad (3.12)$$

Equation 3.12 is the equation for a straight line tangent to the Rowland circle at the normal to the grating. Thus any point on the tangent will be focused vertically and brought to a horizontal astigmatic line on the same tangent.

Equations 3.10 and 3.12 are crucial to the understanding of multiplexing with a spherical grating. They explain why astigmatism is of concern only for demultiplexing and not for multiplexing. To multiplex several different wavelengths into one transmission fiber, the transmission fiber is placed on the Rowland circle normal to the grating. The emitting fibers are placed along the Rowland circle such that their individual emitted wavelengths will form a common image at a point, B, on the face of the transmission fiber. In this case the image angle, β, is equal to zero. The distances from the grating to the image point for both the horizontal focus and the vertical focus are the same since $\cos\beta=1$ makes r' in Equation 3.10 (horizontal focus) and r' in Equation 3.12 (vertical focus) identical. Therefore each emitted wavelength forms a stigmatic image at the point B.

For demultiplexing the transmission fiber is again placed on the Rowland circle normal to the grating. In this case, however, the transmission fiber is the emitter and its position corresponds to the point A with α now equal to zero. The light incident on the grating will be focused and form two images since the location of the point A for horizontal focus (r in Equation 3.10) and vertical focus (r in Equation 3.12) is identical. The locations of the images for horizontal and vertical focus will be different. The locations of the horizontal focal points of the different wavelengths will lie along the Rowland circle. The locations of the vertical foci will lie along a line tangent to the normal of the Rowland circle at the grating normal. It can be seen from Equation 3.10 and 3.12 that the only point where the horizontal and vertical focal points coincide is where $\beta = 0$, the position occupied by the emitting transmission fiber.

The condition for constructive interference of light rays reflected from adjacent diffracting elements (Equation 2.6) is also applicable for spherical gratings. The following expression can be developed [Samson 1967] for the central ray with the use of Equations 3.7 and 3.8

$$(1 + \frac{z^2}{r^2})^{-1/2} (\sin\alpha + \sin\beta_0) = \frac{m\lambda}{a}. \quad (3.13)$$

where (r'_0,β_0,z'_0) is the location of the image point for the ray AOB in cylindrical coordinates. For most gratings, $\frac{z^2}{r^2}<<1$ (e.g. the grating used in thesis has a $\frac{z^2}{r^2}$ value of $\sim$ 0.02) and Equation 3.13 can be rewritten in the form

$$\pm m\lambda = a(\sin\alpha + \sin\beta). \quad (3.14)$$

where a is the ruling separation and α is the angle of incidence and β is the angle of reflection. The negative sign in Equation 3.14 is for "outside" orders. Outside orders are images that are formed between the point where $\alpha = \beta$ on the Rowland circle (the location of the zeroth image) and a tangent to the grating. This can be visualized as the part of the Rowland circle where $\beta>\alpha$. "Inside" orders are images that lie on the Rowland circle between the object point and the zeroth order of the image. In multiplexing β will be zero and inside orders are focused onto the face of the transmission fiber. In demultiplexing α is zero and outside orders are being imaged on the Rowland circle.

A. DISPERSION

The various wavelengths of a source are separated and focused by the grating along the Rowland circle. Each image focused will have a certain distribution of wavelengths present . The dispersion of the grating is a measure of this distribution of wavelengths. For a fixed image, differentiation of Equation 3.14 determines the change in image angle for a change in wavelength.

$$\frac{d\beta}{d\lambda} = \frac{m}{a\cos\beta}. \quad (3.15)$$

The angular dispersion is defined as the quantity $\frac{d\beta}{d\lambda}$. A quantity called the plate factor is more useful in describing grating behavior than angular dispersion. The plate factor is used to calculate the change in wavelength versus the change in distance around the circumference of the circle.

To determine the plate factor it is first necessary to develop an expression for the linear dispersion, defined as $d\lambda/dl$. This is the reciprocal of the plate factor and is related to the angular dispersion as shown by Equation 3.16.

$$\frac{d\lambda}{dl} = \frac{d\lambda}{d\beta}\,\frac{d\beta}{dl}. \tag{3.16}$$

By inspection of Figure 3.3 the relation between the angular change and the change in distance around the circumference of the Rowland circle can be expressed as $R\Delta\beta = \Delta l$.

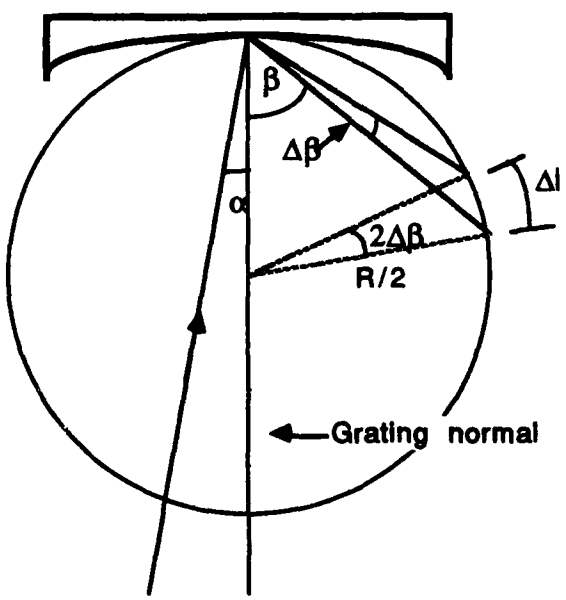

Figure 3.3 Relationship between angular and linear displacement

The expression for the plate factor can be developed by replacing Δ by the differential d in the limit as Δ becomes increasingly small. Using $Rd\beta = dl$ and Equations 3.15 and 3.16 the plate factor can be expressed as

$$\frac{d\lambda}{dl} = \frac{d\cos\beta}{mR}. \tag{3.17}$$

Equation 3.17 gives the change in wavelength for a change in distance along the circumference of the Rowland circle (e.g. nm/mm). A small plate factor represents a large dispersion because a large change in distance is required for a small change in wavelength. From Equation 3.17 it can be seen that dispersion increases with order and decreases as β increases. When multiplexing, $\beta = 0$ and the dispersion is constant. This is not the case for demultiplexing. Using the results of Equation 3.14 it can be shown that β increases with wavelength. Therefore when demultiplexing, longer wavelengths will suffer less dispersion in the image.

B. RESOLVING POWER

The resolution of a grating determines whether distinct wavelengths, differing by a small amount $\Delta\lambda$, can be distinguished from one another. Dispersion determines the separation of the wavelengths. Each wavelength of light forms a diffraction pattern upon reflection from the grating. The angular width of the maxima is dependent on the number of diffracting elements, N. The first zero in the diffraction pattern occurs when $\sin\theta = \lambda/Na$. The phase difference, α, between adjacent rays is π/N and Equation 2.5 is equal to zero. If the angular halfwidth is defined as the angular difference between the location of the maximum ($\sin\theta = m\lambda/a$) and the the adjacent zero ($\sin\theta = m\lambda/a + \lambda/Na$), the width of each maximum will decrease with increasing N, while their location remains constant. The angular halfwidth of a local maximum for a plane grating is

$$\Delta\beta = \frac{\lambda}{Ndcos\beta}. \tag{3.18}$$

The width $\Delta\beta$ is the theoretical limit of the resolution of a grating. The Rayleigh criteria can be used to obtain a more realistic condition for resolution. The Rayleigh criteria for resolution states that two lines of equal intensity will be just resolved when the maximum of one falls on the minimum of the other (Figure 3.4a). The resolving power $\Re$ is defined as $\lambda/\Delta\lambda$, where $\Delta\lambda$ is the minimum wavelength separation which can be resolved. Expressing $\Delta\lambda$ in terms of $\Delta\beta$,

$$\Delta\lambda = \Delta\beta \frac{d\lambda}{d\beta}. \tag{3.19}$$

Using the expressions for angular dispersion, $\frac{d\beta}{d\lambda}$ (Equation 3.15), and angular halfwidth, $\Delta\beta$ (Equation 3.18), an expression for the resolving power, $\Re$, can be developed

$$\Delta\lambda = \frac{\lambda}{mN}. \tag{3.20}$$

Thus the resolving power is

$$\Re = \frac{\lambda}{\Delta\lambda} = mN \tag{3.21}$$

The actual quality of the grating determines whether or not this theoretical limit is achieved.

C. OPTIMUM WIDTH

Equation 3.18 was used in the development of the resolving power. The equation is valid only for a plane grating so the results derived using Equation 3.18 must be modified when using a spherical grating. Equation 3.21 shows that the resolution of a plane grating increases linearly with the number of diffracting elements, N. For a plane grating of constant width this corresponds to an increase in the ruling density (1/a). The

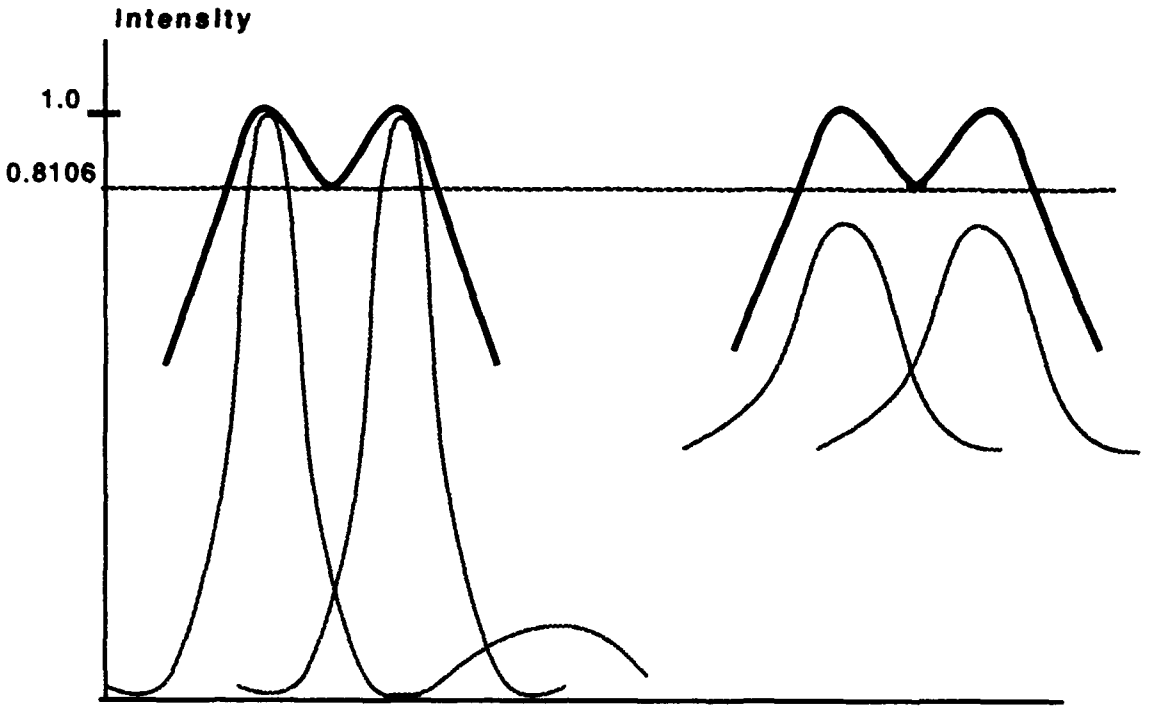

Figure 3.4 Rayleigh criterion (a) for plane gratings (b) for concave gratings

resolution of a concave grating also increases linearly with N, but after a certain point it becomes constant, regardless of the increase in ruling density. The point where resolution becomes constant is determine by the optimum width. The following expression for optimum width, W_{opt}, is taken from Samson [1967].

$$W_{opt} = 2.51\left[R^3\lambda\frac{\cos\alpha\cos\beta}{\sin^2\alpha\cos\beta + \sin^2\beta\cos\alpha}\right]^{1/4}. \qquad (3.22)$$

As an example, the optimum width of a grating with a radius of curvature of 115mm for a wavelength of 780.0nm is ~ 20.9cm. It can be seen that W_{opt} is identical for multiplexing (β=0) and demultiplexing (α=0).

A modified form of Rayleigh criterium applies for concave gratings. The maximum of one line is not required to fall on the first minimum of the other. Instead, two lines of

equal intensity will be just resolved when the wavelength difference between them is such that the minimum total intensity between the lines is $8/\pi^2$ (= .8106) times as great as the total intensity at the central maximum of either of the lines. It can be seen from Figure 3.4 the minimum of the composite structure for both cases of the Rayleigh criteria is the same. Table 3.1 shows the effect of the width of a concave grating on the resolving power.

Table 3.1 RESOLVING POWER OF THE CONCAVE GRATING AS A FUNCTION OF GRATING WIDTH

Width of Grating W	Resolving Power R
$W > W_{opt}/1.18$	$mN = W(m/d)$
$W = W_{opt}$	$0.92W_{opt}(m/d)$
$W >> W_{opt}$	$.75W_{opt}(m/d)$

IV. EXPERIMENT

Recall from Chapter II that astigmatism occurs for any off axis image. When multiplexing, the image of all channels is normal to the grating, hence the effects of astigmatism are negligible. In demultiplexing,however, the image for each channel is off axis and astigmatism is a major factor of system efficiency. Therefore, only demultiplexing was studied as the performance of a high channel system is limited by its ability to demultiplex. The experimental setup to study the possibility of demultiplexing 180 channels was composed of three main components: the light sources, optical fiber and the grating. Each is discussed in further detail below.

A SOURCES

The initial light sources used were light emitting diodes (LEDs) with a wavelength of 660nm and a linewidth of 50nm. The LEDs were connected to the optical fiber with SMA connecters. The nominal launched power from a one meter fiber was 1.5μW. The LEDs proved unsatisfactory because of their low power and broad linewidth. As an alternative, four laser diodes of different wavelengths were used as light sources.

The laser diodes were all equipped with integral PIN photodiodes that monitored the output power of the laser. The output power is a function of the temperature of the device and the forward current. Constant optical power output can be maintained by monitoring the PIN current. Constant PIN current is equivalent to constant optical power. The four sources were all pigtailed into optical fiber. Table 4.1 describes the four sources used in the experiment. All the lasers had a rated power output of 5mW. Pigtailing the laser into optical fiber reduces the usable power as seen in Table 4.1.

Table 4.1 SOURCES

Wavelength	Launched power	PIN current
780.0 nm	1mW	385μA
789.0 nm	1mW	557μA
848.0 nm	.785mW	395μA
849.0 nm	.830mW	390μA

B. FIBER

The fiber used was 50/125μ graded index multimode fiber. The numerical aperture (NA) of the fiber was 0.24. This determines the acceptance cone of the fiber and the divergence angle of light transmitted at the fiber face. A large acceptance cone is not required for optical fibers used in demultiplexing due to the focusing properties of the spherical grating. A small acceptance cone also reduces the amount of crosstalk. Crosstalk occurs when light that is imaged on the face of one optical fiber falls within the acceptance cone of an adjacent fiber. A small divergence angle limits the spread of emitted light and more light will be incident on the grating at a given distance.

C. GRATING

The grating was the critical component of the multiplexing system. Table 4.2 contains the specifications of the grating. The efficiency of the grating is maximized at the first order of the blaze wavelength and drops off at other wavelengths. Figure 4.1 shows the grating response at the blaze wavelength. This figure clearly shows that the intensity of the first order is maximized when the grating is illuminated at the blaze wavelength.

Table 4.2 GRATING SPECIFICATIONS

Grooves/mm		600
Radius (concave)		115 mm
Blaze wavelength		4267Å
Blaze angle		$7^0 21'$
Ruled area	Width	Length
	30 mm	28mm

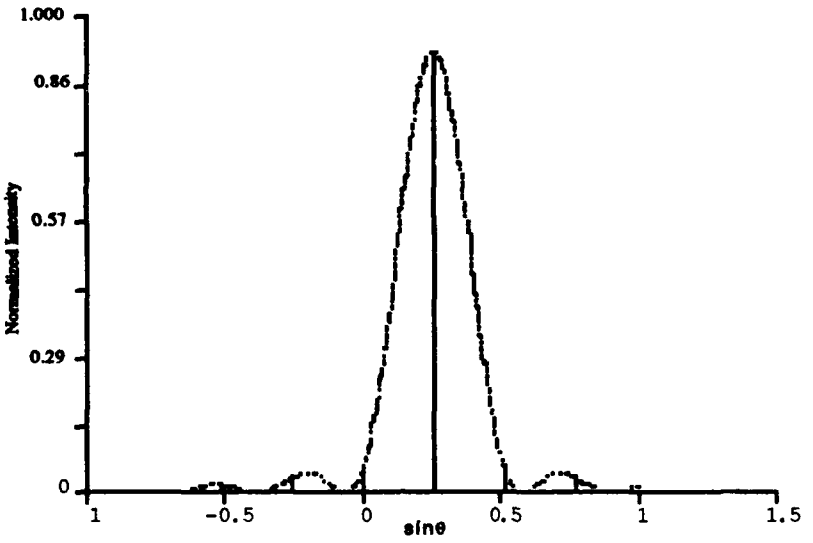

Figure 4.1 Calculated Blazed Grating Irradiance λ=426.7nm

For wavelengths other than the blaze wavelength, two effects occur. First, the angular locations of the principal maxima will shift because of their dependence on wavelength. The first order intensity of longer wavelengths will occur at greater values of $\sin\theta$ and the relative spacing between orders will increase as well. Secondly, while the location of the envelope defined by $\text{sinc}^2\beta$ will remain centered where $\sin\theta$ is equal to $\frac{\lambda_{blaze}}{a}$, the relative width of the envelope will increase. The zeroes of the $\text{sinc}^2\beta$ function occur where $\sin\theta$ is equal to λ/b. As the wavelength increases, the spacing between zeroes will increase. The net result of these two effects can be seen in Figures 4.2 through 4.4. These figures show the intensity curves over a range of wavelengths representative of the envisioned 180 channel multiplexer. As the wavelength increases the intensity of the first order is reduced because it is located further away from the maximum of the envelope and the broadening envelope tends to effect all orders equally.

It can be seen in Figure 4.2 that the position of the first order maximum has increased and that zeroes of the $\text{sinc}^2\beta$ function are more widely separated. Figure 4.3

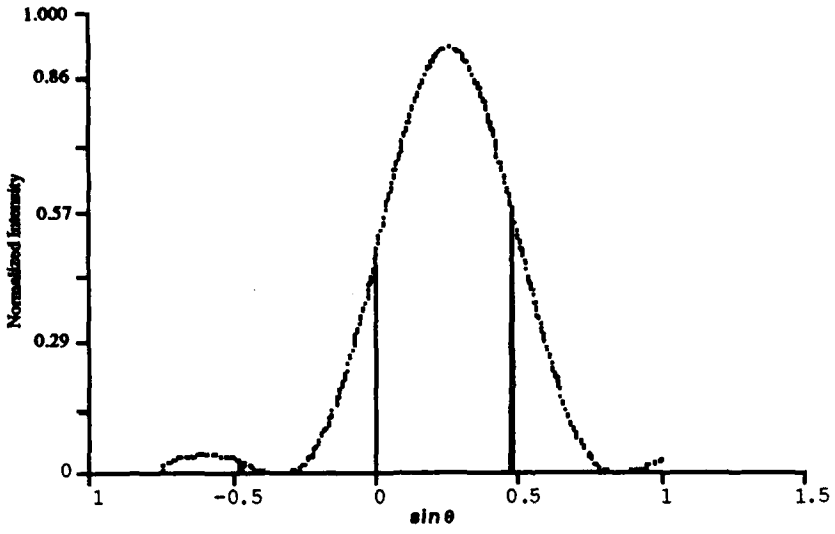

Figure 4.2 Calculated Blazed Grating Irradiance λ=789.0nm

shows the grating response at a wavelength equal to nearly twice the blaze wavelength. At this wavelength the intensity of the first order maximum and the zeroth order are almost equal. Figure 4.4 shows that at wavelengths greater than twice the blaze wavelength the intensity of light in the zeroth order is greater than the intensity present in the first order. This decreases the usefulness of the grating as light in the zeroth order is composed of all wavelengths and cannot be used in multiplexing.

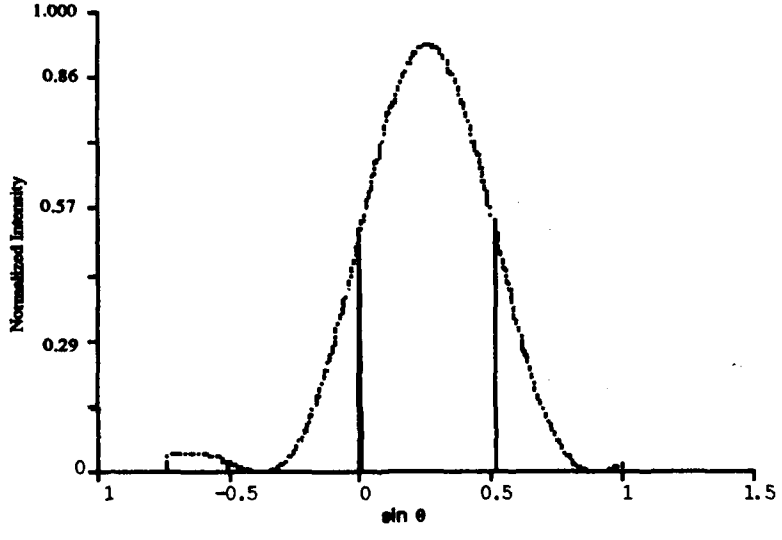

Figure 4.3 Calculated Blazed Grating Irradiance λ=849.0nm

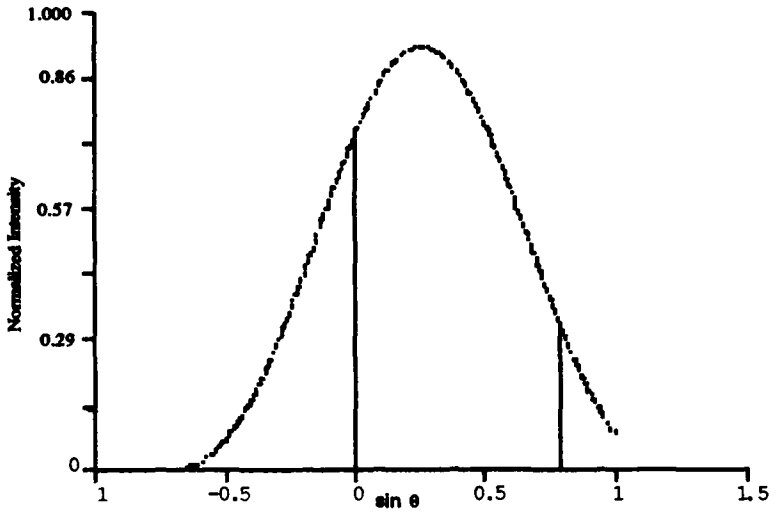

Figure 4.4 Calculated Blazed Grating Irradiance λ=1307.0nm

The efficiency of a grating at a specific wavelength is defined as the intensity of light in the first order divided by the intensity of light present in all orders. The calculated efficiencies of the grating at the wavelengths of interest are listed in Table 4.3.

Table 4.3 GRATING EFFICIENCY VS WAVELENGTH

Wavelength	Efficiency
426.7 nm	.877
780.0 nm	.650
789.0 nm	.524
848.0 nm	.490
849.0 nm	.490
1307.0 nm	.295

The radius of the grating is important because it determines the size of the Rowland circle used for multiplexing and the the plate factor. The plate factor for this grating can be calculated using Equation 3.17 Only first order maxima will be used as the efficiency of the grating is maximized for first order.

$$\frac{d\lambda}{dl} = \frac{a\cos\beta}{mR} \quad = 14.5 \text{ nm/mm.}$$

The plate factor determines the linear separation of two images of different wavelengths that are focused on the Rowland circle. As stated in Chapter II, this distance is measured along the circumference of the Rowland circle.

D. PROCEDURE

The experimental setup was designed to simulate demultiplexing. To this end,the input fiber was fixed in position in line and normal to the center of the grating, on the Rowland circle. The input fiber's position corresponded to point A in Figure 4.5, with the angle of incidence, α, equal to zero. The grating was mounted in an holder to maintain the geometry between the input fiber and the grating. The only free element in the system was the output fiber which was mounted on an XYZ translator to allow for alignment and adjustments required when changing source wavelengths.

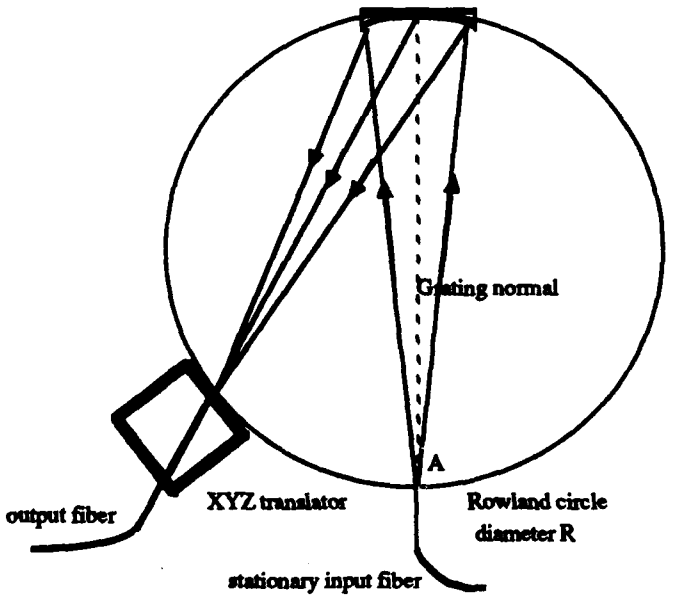

Figure 4.5 Experimental setup for demultiplexing

The light incident on the grating was reflected and focused onto the end of a single output fiber. The fiber was a 50/125μ graded index multimode fiber. The output fiber had

an SMA connector on the end and could be connected either to a photodiode or the detector of an optical power meter. The photodiode had a fast response and was used to align the fiber and to make measurements of the image at various points in the horizontal focal plane. The voltage response of the photodiode was proportional to the intensity of the light incident on the photodiode. The power meter, on the other hand, had a slow response time and was used only to measure the absolute intensity of the emitted light and the intensity of light transmitted by the output fiber.

The output fiber was positioned to maximize the voltage response of the photodiode. The voltage of the photodiode was monitored with an oscilloscope. An oscilloscope was used for system alignment because it was easier to visually monitor the photodiode response using the oscilloscope display. Once the output fiber had been correctly positioned, the voltage of the photodiode was read with a digital multimeter to improve accuracy. The voltage readings of the photodiode as a function of the output fiber position in the horizontal focal plane were used to construct image patterns as discussed in the next chapter. Coupling efficiency was calculated by dividing the intensity emitted by the input fiber by the intensity launched by the output fiber. Both of these intensities were measured using the optical power meter.

All data in the experiment were taken with the sources at constant power, however. coupling was achieved when the source power was modulated. This demonstrated the ability to use digital processing to carry the information in the data channels. The data rate would be limited by the modulation limit of the laser diode.

V. RESULTS

The linewidth and power of the laser diodes were measured in order to more accurately interpret the results of the experiment. The optical power of a laser diode is dependent on the current supplied to the device and is constant for a given PIN current. Therefore power measurements are referenced to a specific PIN current. Table 5.1 shows a comparison of the measured and expected laser diode powers for the four sources used. The power of the 780.0nm diode was not measured due to a premature failure of this device. The diodes were tested at the same stated PIN currents as listed in Table 4.1.

Table 5.1 LAUNCHED POWER VS WAVELENGTH

Wavelength	Stated power	Measured power
780.0 nm	1mW	not measured
789.0 nm	1mW	.618mW
848.0 nm	.785mW	.665mW
849.0 nm	.830mW	.714mW

None of the sources achieved the stated power levels Care was taken to rule out systematic errors. For example, the active area of the detector used to measure optical power was larger than spot size of the emitted radiation on the face of the detector, therefore no light was lost in detection. The end faces of the optical fibers were carefully cleaved to maximize the light output and ensure the proper transmission pattern . The measured powers were used in all calculations of efficiency.

A. LINEWIDTH

The number of channels that can be multiplexed using the same source is dependent on the linewidth. The linewidth of the sources were determined using the image patterns. The image width is a result of the convolution of the linewidth of the source and the resolution of the grating. The resolution of the grating was discussed in Chapter III.

Using Equation 3.22, the optimum width of the grating was calculated to be approximately 21 mm for the range of wavelengths used (780nm - 849nm) The grating had a width of 30mm The case where $W=W_{opt}$ from Table 3.1 was used to modify the theoretical resolution. The average resolution of the grating was 0.07 nm.

The width of the image pattern is defined as the distance between the full width at half maximum (FWHM) of the points of the image voltage as a function of distance (measured horizontally along the Rowland circle). The plate factor can be used to convert distance on the Rowland circle to an equivalent change in wavelength. The change in distance between the FWHM points can then be represented as a change in wavelength. The widths of the images were on the order of several nanometers. The average resolution was at least an order of magnitude smaller than the change in wavelength across the width of the image. In the convolution of the resolution and linewidth, the effect of the resolution on the image can be ignored. Therefore, the linewidth of the source can be calculated from the width of the image. Table 5.2 shows the calculated linewidths of the source.

Table 5.2 SOURCE LINEWIDTH

Wavelength	Linewidth
780.0 nm	1.47 nm
789.9 nm	1.66 nm
848.0 nm	3.20 nm
849.0 nm	3.27 nm

Figure 5.1 shows three linewidth measurements of the 780.0nm source. As can be seen from Figure 5.1, there were no appreciable differences between the three measurements. Figure 5.2 shows the image pattern of the 849.0nm source. This clearly shows the Gaussian nature of these linewidths.

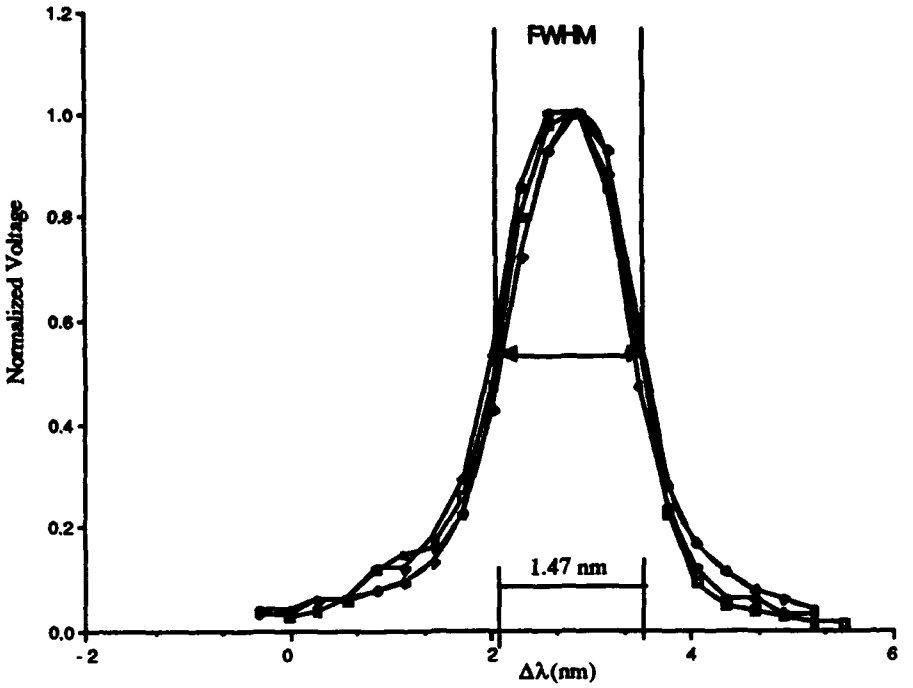

Figure 5.1 Linewidth of 780.0nm Source

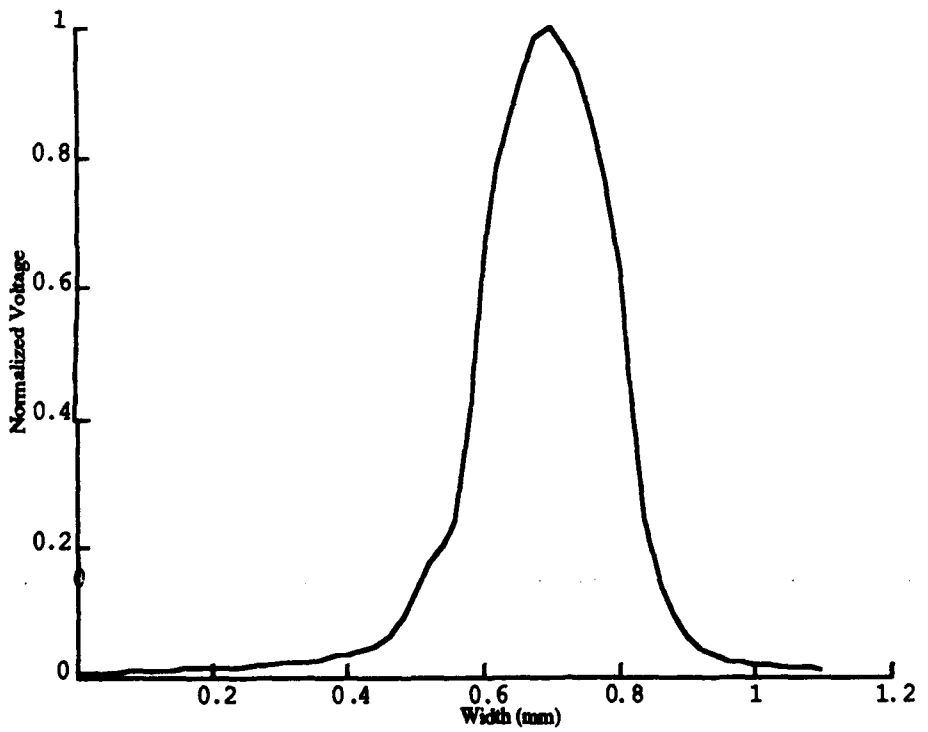

Figure 5.2 Image Width at Horizontal Focus λ=849.0nm

The linewidth and wavelength of the light emitted by laser diodes depends on the power level. The center wavelength and linewidth both increase as the output power increases. Figure 5.3 shows the image width of the 789.0nm source driven at a significantly higher power. The linewidth is approximately 7.85 nm which is almost five times the value calculated in Table 5.2. A shift in wavelength is also expected at these higher powers. Unfortunately this shift cannot be determined as only relative detector positions were recorded. The launched power of the source used in Figure 5.3 was .716mW as compared to .618mW from the same source in Table 5.1. The increase in wavelength and linewidth are expected from the data presented in Figure 5.4. These data are for a laser diode at 780.0nm but are typical for laser diodes of any wavelength.

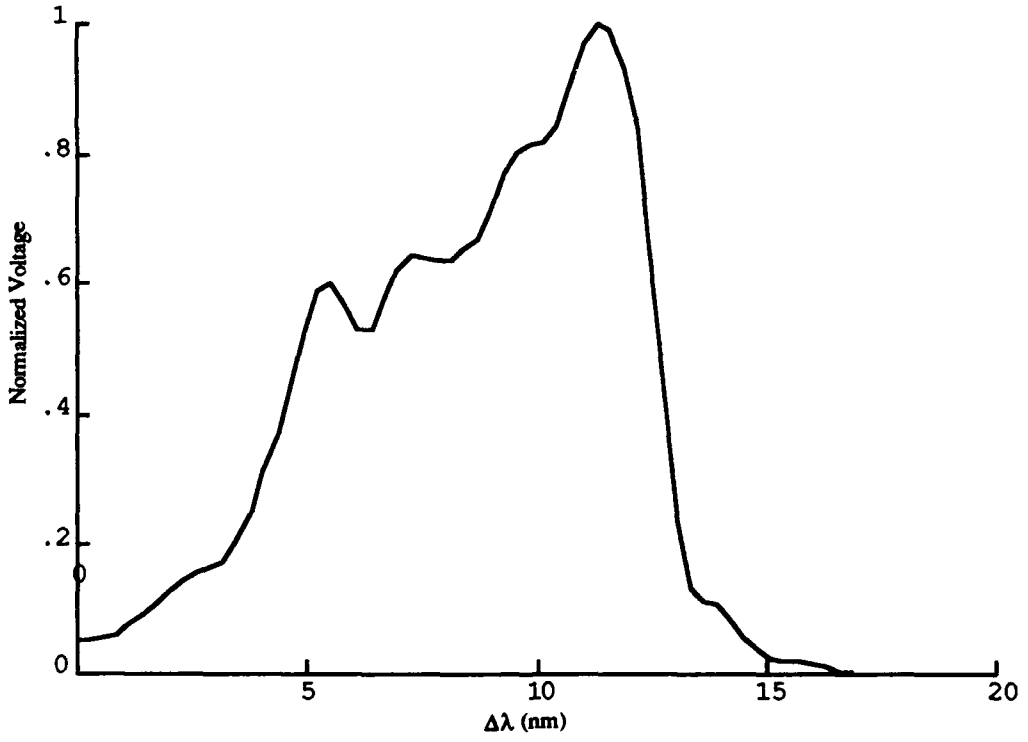

Figure 5.3 Image Width at Horizontal Focus λ=789.0nm

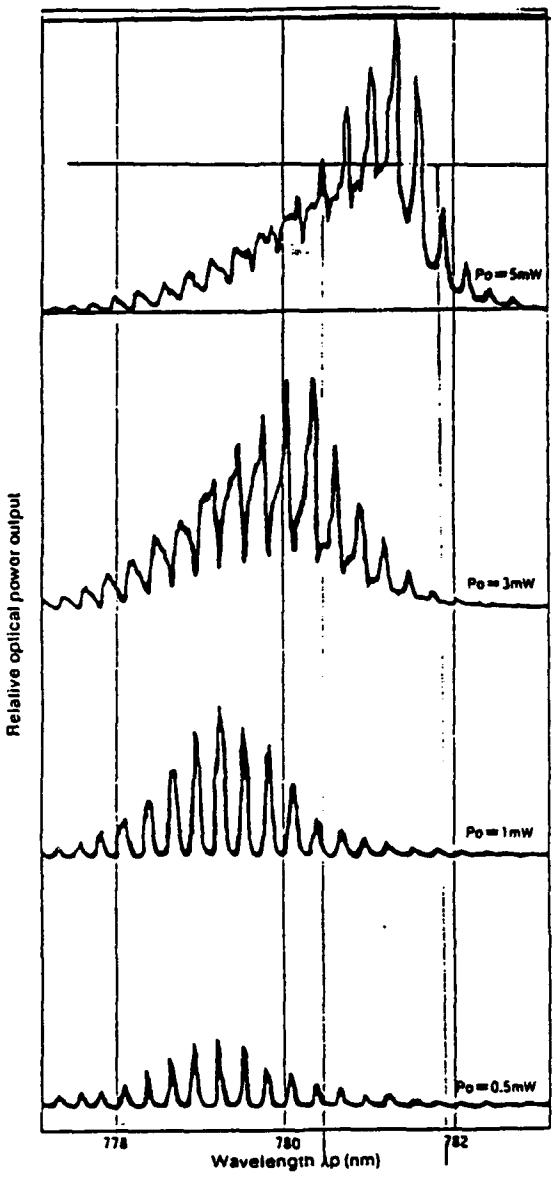

Figure 5.4 Optical Power Output Dependence of Wavelength
(from Sharp Corp. data sheet for LT023MS)

B. EFFICIENCY

The coupling efficiency of the demultiplexer system is defined as the ratio of the received power to the transmitted power. The transmitted power is the power launched into the output fiber. These were measured previously for the four laser diodes and appear in Table 5.1 The light emitted by the output fiber is reflected and focused by the grating onto

the face of the receiving optical fiber. This incident light travels through the optical fiber and is measured at the other end. The power of the light emitted at this end was measured by the optical power meter and represents the received power of the system. The optical power meter was used for both measurements to avoid conversion errors from two different measuring techniques. The coupling efficiencies of the system are listed in Table 5.4

Table 5.4 EFFICIENCY VS WAVELENGTH

Wavelength	Efficiency
780.0 nm	not measured
789.0 nm	.0002
848.0 nm	.0003
849.0 nm	.0003

The low efficiency of the system at all wavelengths used is the result of three factors: the grating efficiency, NA mismatch between the fiber and the grating, and astigmatism. Of the three factors, astigmatism is the most detrimental to the efficiency of the system and the hardest to correct.

The grating efficiency at various wavelengths has previously been calculated in Table 4.3. Blazing the grating at a wavelength closer to the wavelengths used in the experiment would approximately double the efficiencies of Table 5.4. As stated previously, the numerical aperture of the fiber is .24. This divergence cone forms a circular spot of $2583mm^2$ on the face of the grating. The grating has an area of only $720mm^2$. Assuming uniform illumination, 72% of the incident light is lost due to this mismatch. Thus by increasing the size of the grating, the efficiencies of Table 5.4 could be increased by over a factor of three.

C. ASTIGMATISM

Astigmatism is the primary factor controlling coupling efficiency. The low efficiency of a demultiplexer system is due to the pattern of the image formed at the horizontal focus point. The image is a vertical line. Recall that the horizontal focus is used to reduce crosstalk. The width of the image is minimized, but the height is not.

The image heights at horizontal focus were measured in the same manner as the image widths at horizontal focus. The image height of the 849.0nm source is shown in Figure 5.4 The FWHM value of the image height is 4.21mm. The width of the image at horizontal focus has a FWHM value of 0.23mm. The image at the horizontal focal point is nearly 20 times larger in height than width.

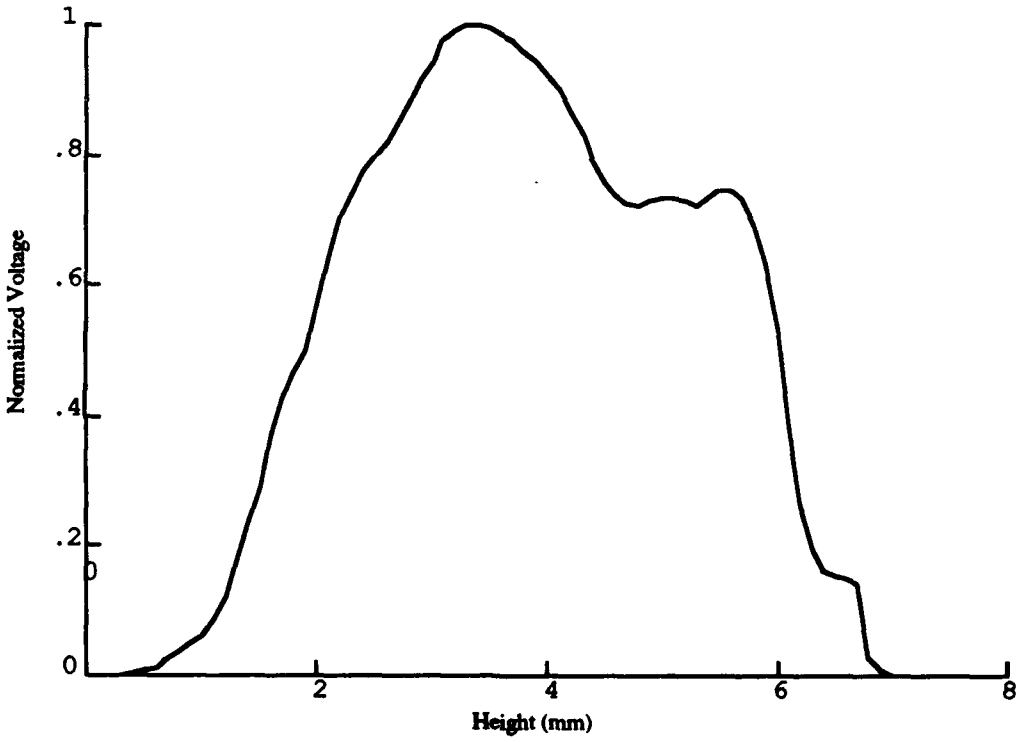

Figure 5.4 Image Height at Horizontal Focus λ=849.0nm

The two arrays representing height and width as functions of position can be multiplied to form a three dimensional surface representation of intensity. Figure 5.5 shows a scale representation of the image of the 849.0 nm source. This figure clearly shows the extent to which the image is spread out on the vertical direction.

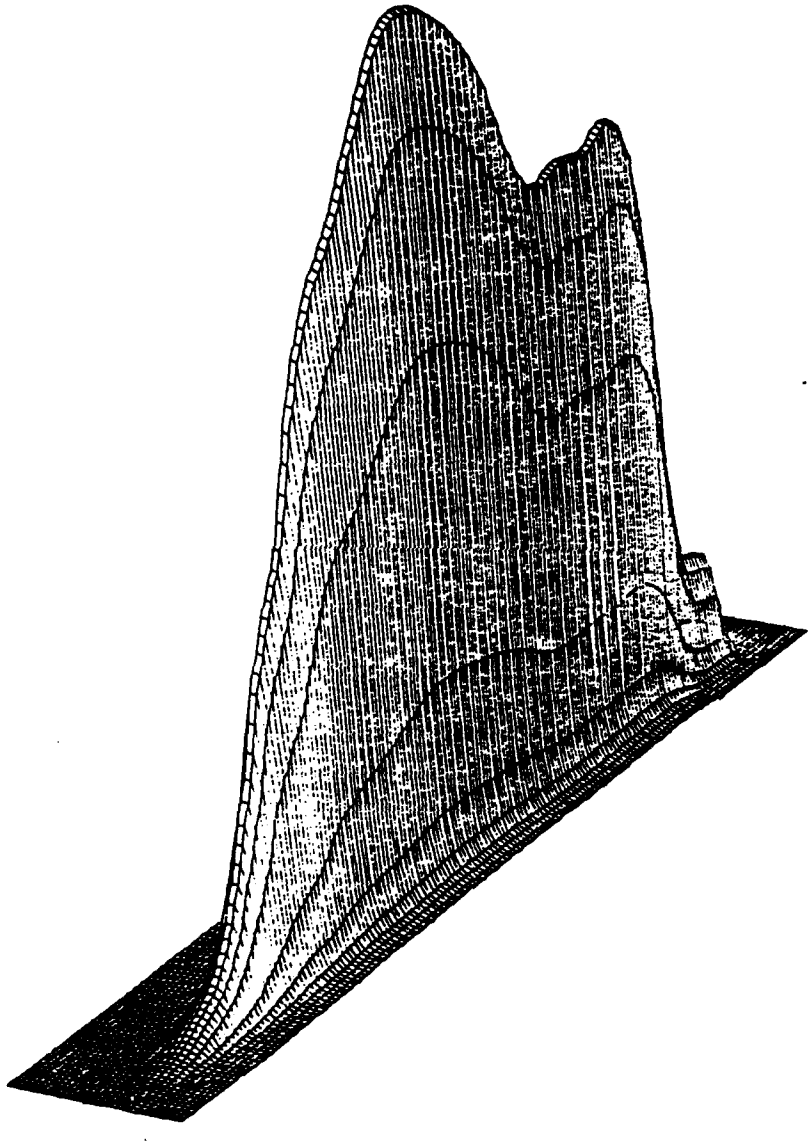

Figure 5.5 Scale Representation of Image at Horizontal Focus λ=849.0 nm

In order to evaluate the effect of astigmatism on the coupling efficiency, a contour plot of the image intensity at the horizontal focus a function of change in position in the horizontal focal plane is shown in Figure 5.6. Note that different scales were used on the two axes to preserve the detail of the plot. The loss in efficiency due to the mismatch between image size and fiber area can be calculated by determining the fraction of the intensity in the image that is coupled into the fiber. By superimposing the area of the fiber on the intensity contour and integrating the underlying intensity, the power of the light coupled into the fiber can be calculated. The intercept ratio is defined as the power coupled to the fiber divided by the total power of the image. The intercept ratios for three sources are listed in Table 5.4. The values are similar and explain why astigmatism is the predominant factor in the low coupling efficiency of a spherical grating demultiplexer. Correction of blaze angle and numerical aperture mismatch will at best increase the coupling efficiency by a factor of six, whereas astigmatism correction yields an increase in the coupling efficiency of nearly 500.

Table 5.4 INTERCEPT RATIO VS WAVELENGTH

Wavelength	Intercept Ratio
789.0 nm	.0017
848.0 nm	.0022
849.0 nm	.0019

By combining the three factors of NA mismatch, grating efficiency and intercept ratio, an estimate of the coupling efficiency can be made. This is compared to the measured efficiency determined by the optical power meter. The results for the three wavelengths used are contained in Table 5.5.

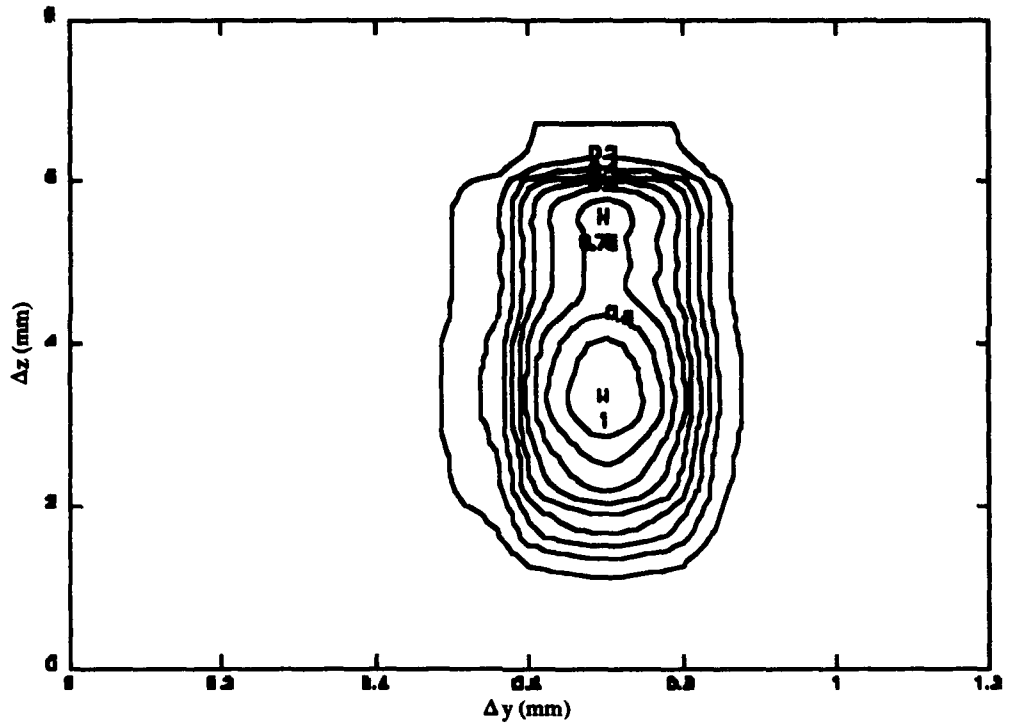

Figure 5.6 Normalized Voltage Contour for Image at Horizontal Focus λ=849.0nm

Table 5.5 *COUPLING EFFICIENCY VS WAVELENGTH*

Wavelength	Calculated	Measured
789.0 nm	.0002	.0003
848.0 nm	.0003	.0004
849.0 nm	.0003	.0003

There is good agreement between the calculated and measured efficiencies. The largest source of error in the calculated efficiency is in the determination of the intercept ratio. The grating efficiencies and numerical aperture mismatch were calculated numerically and are not effected by experimental error. The measured coupling efficiencies were calculated using the ratio of two power measurements which reduced the effect of any systematic error.

D. CHANNEL DENSITY

At this point it is possible to estimate the number of channels that can be multiplexed with the present design. The shortest wavelength used in the design was

780.0nm. The second order of the 780.0nm source will overlap the first order intensity of a 1560.0nm source. Since it is impossible to separate the intensity due to each source from the total intensity of the image, images from sources whose wavelengths are greater than 1560.0nm will be contaminated with higher orders. It may be that the intensity of the overlapping higher orders in an image are weak enough to be considered negligible compared to the intensity of the first order. However, for the sake of simplicity, the condition of non-overlapping maxima will be used. Thus the upper limit of the wavelength range will be set at 1560.0nm

The maximum channel capacity for the experimental setup can be estimated by examining Figure 4.5. For demultiplexing, the input fiber is normal to the grating at the point A. The reflection angle, β, of the first order image for incident light at a wavelength of 780.0nm is calculated using Equation 3.14 to be approximately 28°. Similarly, the longest wavelength required to be focused, 1560.0nm, will have a reflection angle, β, of 69°. From Chapter III, the arc length, l, on the Rowland circle between the shortest wavelength and longest wavelength images can be calculated from the expression $R\Delta\beta=\Delta l$ and is equal to 83.3mm. Assuming equal linear separation for 180 channels over the range of 780.0nm, the fibers centers would be separated by 0.46mm. This separation is easily achievable using 125μ fibers.

VI. CONCLUSIONS

A. SUMMARY OF FINDINGS

Demultiplexing was demonstrated using four different wavelengths:780.0nm, 789.0nm, 848.0nm and 849.0nm. Demultiplexing was possible with a coupled power 35dB lower than the source power. The losses in the coupled intensity were due to three factors: the grating efficiency, the numerical aperture mismatch between the optical fiber and the grating, and astigmatism. Multiplexing should be possible with negligible losses because stigmatic images are formed.

The coupling efficiency of the design can be improved by correcting the three factors affecting the efficiency of demultiplexing. The first improvement would be to blaze the grating at a wavelength closer to the range of wavelengths used. Blazing at the center wavelength of the range used in the system would be an acceptable design compromise. Demultiplexing in this study was accomplished with grating efficiencies as low as 49%.

The second improvement to the design would be to match the numerical aperture of the fiber to the area of the grating. This can be accomplished either by using a fiber with a different numerical aperture or increasing the size of the grating. Fiber numerical apertures are available from 0.10 to nearly 1.0. The greater the numerical aperture, the greater the power a laser diode can couple into a pigtailed fiber for transmission. Therefore it would be better to increase the size of the grating before reducing the numerical aperture when matching the two elements.

Aberration correction represents the most difficult improvement to make, but has the greatest effect on the coupling efficiency. Aberration correction requires the manufacture of a grating using a highly specialized ruling engine and would dramatically increase the price of a system. The effects of aberration can be reduced using larger

diameter fibers to increase the intercept ratio. If light detectors could be manufactured on the order of the image size, they could replace optical fibers. Photodetectors used in some optical instruments are on the order of 50μ wide, but are mounted on a plane surface. The mounting surface would have to be curved to match the Rowland circle for a demultiplexer. As this is not yet possible, a specialized grating represents the most promising direction to increase coupling efficiency.

The challenge yet to be met in multiplexing 180 channels is not in the design of the system itself, but in the sources used. Distinct sources for each of the 180 wavelengths are not required as wavelength slicing can be used to form 180 channels [Rome Air Development Center Technical Report 83-146, June 1983]. The wavelength range of the system (780nm-1560nm) cannot be covered by existing light sources. The wavelength range need not be as great as 780nm if the wavelength separation of channels is less than 4nm. However, even for a wavelength separation as low as 1nm significant gaps will occur in the source coverage of the system's wavelength range.

B. RECOMMENDATIONS FOR FURTHER STUDY

This thesis evaluated the possible design of a 180 channel multiplexer. The multiplexer was not actually built so several areas of concern would have to be addressed to construct a functioning prototype. With 180 channels spanning a wavelength range of 780.0nm, alignment of the system would be crucial. It might be very difficult in practice to properly align 180 channels and then maintain that alignment under operating conditions.

There are some problems that are related to the use of laser diodes as light sources. The laser diodes require special power supplies to operate properly. Pigtailed laser diodes would be difficult to replace and might require realignment of the system, depending on how closely the replacement diode matches the original in wavelength. Some form of

temperature stabilization of the system would be necessary to prevent temperature induced changes in the diode's emitted wavelength.

The significant area which has not been investigated in this thesis is the actual design of a rotary joint. The joint would have to maintain a rotating fiber in the correct axial alignment. Close tolerances would be required to do this for 125μ fibers. The use of small lenses, such as GRIN lenses, to change the emitted light into plane parallel rays for transmission across the rotational interface could be investigated as a means of reducing the accuracy necessary for a fiber optic rotary joint.

Once the necessary coupling efficiency has been obtained for 180 channels, other problems relating to the data transfer can be addressed such as the bit error rate and the modulation frequency required to transmit the information received by the detectors. The solutions to these problems might be different in the case of WDM as opposed to TDM.

BIBLIOGRAPHY

Aoyama, K., and Minowa, J., "Low-loss Optical Demultiplexer for WDM systems in the 0.8mm Wavelength Region",*Applied Optics*, v. 18, no. 6, pp 2834-2836, 15 Aug 1979.

Aoyama, K., and Minowa, J., "Optical Demultiplexer for a Wavelength Division Multiplexing System",*Applied Optics*, v. 18, no. 8, pp 1253-1258, 15 Apr 1979.

Fujii,Y., and Minowa,J.,"Optical Demultiplexer using a Silicon Concave Diffraction Grating", *Applied Optics*, v. 22, no. 7, pp 974-978, 01 Apr 1983.

Harada,T., and Kita,T., "Use Of Aberration-Corrected Concave Gratings in Optical Demultiplexers", *Applied Optics*, v. 22, no. 6, pp 819-825, 15 Mar 1983.

Hecht,E., *Optics*, 2nd ed.,Addison-Wesley Publishing Co.,1987

Hendricks, H.D., "Wavelength Division Multiplexing", *SPIE*, v. 512, pp 130-145, 1984.

Jenkins,F.A., and White,H.E., *Fundamentals of Optics*, 4th ed., McGraw-Hill Book Co., 1976.

Lipson, J., and Harvey, G., "Low Loss Wave Division Multiplexing (WDM) Devices for Single Mode Systems", *Journal of Lightwave Technology*, v. LT-1, no.2, pp387-389, Jun 1983.

Minowa, Y., and Minowa, J., "Cylindrical Concave Diffraction Grating Utilizing Thin Silicon Chip", *Electronics Letters* , v.17, no. 24, pp 984-986, 26 Nov 1981.

Rome Air Development Center Technical Report 83-146, *Grating Demultiplexer Study*, by T.L. Mikes and R.A. Shafer, Jun 1983.

Samson,J.A.R., *Techniques of Vacuum Ultraviolet Spectroscopy*, John Wiley & Sons, 1967.

Tanaka, T., Kishi, S., and Tsutsumi, T., "Fiber-optic Multifunction Devices Using a Single GRIN Rod Lens for WDM Transmission Systems",*Applied Optics*, v. 21, no. 19, pp 3423-3429, 1 Oct 1982.

Tanaka, T., Serizawa, H., and Tsujimoto, Y., "Simple Structure High Isolation Multi/Demultiplexer", *Electronics Letters* , v.16, no. 23, pp 870-871, 6 Nov 1980.

Tomlinson,W.J., and Lin,C.,"Optical Wavelength-Division Multiplexer for the 1 to 1.4mm Spectral Region", *Electronics Letters* , v.14, no. 11, pp345-347,25 May 1987.

Tomlinson,W.J., "Wavelength multiplexing in multimode optical fibers", *Applied Optics*, v.16, no. 8, pp 2180-2194, Aug 1977.

Watanabe,R., and Nosu,K., "Optical Demultiplexer Using Concave Grating in 0.7-0.9 mm Wavelength Region", *Electronics Letters* , v.16, no. 3, pp106-108, 31 Jan 1980.

Watanabe,R., and Nosu,K., "Slab Waveguide Demultiplexer For Multimode Optical Transmission in the 1.0-1.4mm Wavelength Region",*Applied Optics*, v. 19, no. 21, pp 3588-3590, 1 Nov 1980

Watanabe,R., Nosu,K., and Fujii, Y., "Optical Grating Multiplexer in the 1.1 to 1.5mm Wavelength", *Electronics Letters* , v.16, no. 3, pp108-109, 31 Jan 1980.

INITIAL DISTRIBUTION LIST

	No. Copies
1. Defense Technical Information Center Cameron Station Alexandria, Virginia 22304-6145	2
2. Library, Code 0142 Naval Postgraduate School Monterey, California 93943-5100	2
3. Dr. K. E. Woehler, Chairman Physics Department Naval Postgraduate School Monterey ,California 93943-5000	1
4. Dr. D. D. Cleary Physics Department, 61-Cl Naval Postgraduate School Monterey ,California 93943-5000	1
5. Dr. Alfred W. M. Cooper Physics Department, 61-Cr Naval Postgraduate School Monterey ,California 93943-5000	1
6. Commander, Naval Sea Systems Command Attn: CAPT J. Paine, Code SEA 06W4; PMS-421 Washington DC 20363-5100	1
7. Commander, Naval Sea Systems Command Attn: Julius Horvath, Code SEA 06W4; PMS-421 Washington DC 20363-5100	1